# An active metamaterial cell concept for nonreciprocal vibroacoustic transmission

**Marin Jalšić[1,*], Neven Alujević[2], Tonko Garma[3], Ivan Ćatipović[2], Marko Jokić[2], Hinko Wolf[2]**

[1] AVL-AST d.o.o., Zagreb

Strojarska 22, 10000 Zagreb, Croatia

[2] University of Zagreb, Faculty of Mechanical Engineering and Naval Architecture,

Ivana Lučića 5, 10002 Zagreb, Croatia

[3] University of Split, Faculty of Electrical, Mechanical Engineering and Naval Architecture,

Ruđera Boškovića 32, 21000 Split, Croatia

*e-mail: marin.jalsic@gmail.com

## ABSTRACT

The challenge of inducing stable and robust nonreciprocal transmission of sound is seen as an important milestone on the path towards developing active acoustic metamaterials. Structures that can transmit sound or vibration in a nonreciprocal manner may be considered as analogous to an electrical diode and could be useful in many applications, such as noise control and the development of invisible acoustic sensors and acoustic cloaking. This paper focuses on the conceptual development and experimental validation of an active metamaterial cell that does not obey the reciprocity principle. The structural cell considered, when activated, significantly attenuates vibration transmission through it in one direction and increases it in the opposite direction. The effect is present in a broad frequency band. The loss of reciprocity is induced by using two concurrent velocity feedback loops with non-collocated sensor-actuator pairs. Inertial accelerometers with time-integrated outputs are used in conjunction with miniature electrodynamic force actuators. The study is first carried out theoretically, using an electromechanically fully coupled lumped parameter model of an otherwise flexible active structure. The derived model is used to conduct analysis of the control system stability and performance. Given that a non-collocated transducer arrangement is considered, special attention is paid to the selection of parameters of the passive system which ensure satisfactory gain margins when the system is made active. In fact, criteria for unconditional stability are derived analytically, in terms of two simple inequalities for the system with idealised sensor-actuator pairs. For realistic transducers, however, unconditional stability is not possible. Nevertheless, if the two inequalities are respected, useful gain margins of the active system can be expected. This is validated experimentally using a dedicated 3D-printed measurement test rig. A substantial reduction of vibration transmission in the desired direction, accompanied by an increase in the opposite one, is recorded experimentally. These results suggest that the control scheme proposed could be used to design an active acoustic metamaterial, which would enable the significantly different transmission of sound depending on the direction it enters such a system.

**Keywords**: active vibration control, dynamic reciprocity, active metamaterials, stability of active control systems, performance of active control systems

# 1 Introduction

The reciprocity principle dictates that if points of excitation and response of a vibrating structure are switched, the measured quantity will not change. In other words, the same frequency response function (FRF) is obtained between the measured quantity and the excitation regardless of the switching [1]. Reciprocity normally holds for passive, linear time-invariant (LTI) systems. It is often a useful property in general modal analysis [1], when obtaining transfer functions for NVH (Noise, Vibration and Harshness) applications in the automotive industry [2], or for obtaining the mass density and the compressibility of soil from measured data in inverse seismic problems [3].

However, circumvention of the reciprocity principle can be equally useful, for example when seeking to isolate or protect a region of space allowing wave transmission in one direction yet blocking it in the opposite one [4]. A great amount of recent research has been carried out in various areas of physics and material science with the aim of developing materials, devices or structures that do not obey the reciprocity principle [4–6], for example in the field of active electromagnetic metamaterials [7], which could be used to propagate microwaves in one direction and block them in the opposite direction. In the field of vibroacoustics, such concepts are interesting for prospective applications such as invisible acoustic sensors [8], acoustic cloaking devices [9], vibration isolation [10], autonomous and active guiding of sound beams [11], or full-duplex sound communication where acoustic waves can be transmitted and received from the same transducer on the same frequency channel [12]. A useful review of approaches to induce nonreciprocity in acoustic and elastic materials can be found in [13]. Such approaches have been mainly proposed in an effort to extend the physical limits on the available choices of acoustic parameters of metamaterial structures [14,15] imposed by their passivity, linearity or time-invariance. In particular, frequency response functions of a passive, linear, and time-invariant medium are bounded by the Kramers-Kronig relations. These relations are a consequence of causality and connect the real and imaginary parts of the medium's FRFs [16].

On the other hand, the passivity in vibroacoustics is strongly related to the damping characteristics of the media involved and the corresponding energy losses. Damping causes attenuation of waves characterised by a relatively high wavenumber. For example, waves shorter than the characteristic thickness of a metastructure, or, in fact, of any structure with cellular inclusions such as porous media or sound absorbing foams, are significantly attenuated during propagation. The beneficial properties of passive resonant metamaterial structures are also often limited to certain frequency bands [17,18]. The width of those bands tends to scale with the scale of the inclusions within the metamaterial [14].

For these reasons, there has been a growing effort to explore active acoustic metamaterials, which could potentially overcome the challenges described above and increase their effectiveness.

Active unit cells of metamaterials with unusual acoustic properties have been considered in several designs [11,19,20]. The term 'active' is employed to point out inclusions within the metamaterial that are able to provide energy to the impinging wave and feedback to the acoustic system, which may be controlled or which are externally biased [14]. For example, nonreciprocal effects in lumped parameter [21] or distributed parameter [22] mechanical structures may be induced by generating tuneable bandgaps. The frequency of these bandgaps can be made tuneable by an active control system which affects the stiffness in the unit cell of the structure. In such a case, the gain of the feedback loop used to tune the stiffness can also be made harmonically time-varying which effectively modulates the resonance frequency of an inner resonant metamaterial. This results in a parametrically excited system that propagates waves in a non-reciprocal manner. By choosing an appropriate modulation frequency, complete unidirectional band gaps have been demonstrated theoretically [21].

With respect to using active metamaterials to achieve unidirectional sound transmission, Fleury et al. [8] investigated an active metamaterial cell that is entirely transparent to tonal sound propagating through it from left to right and highly reflective to sound propagating in the opposite direction. In order to achieve this, a pair of loudspeakers was placed in a 1D acoustic waveguide (rectangular pipe) at a subwavelength distance. The left (absorbing) loudspeaker was shunted with a passive electrical circuit, whereas the right (lasing) loudspeaker was shunted with a carefully tuned non-Foster electrical circuit (negative impedance circuit) [23]. Therefore, the system was made active without the use of sensors or feedback loops, and the authors clearly demonstrated the feasibility of an acoustic sensor invisible to a 250 Hz tone. This active metamaterial cell is based on the concept of parity-time ($\mathcal{PT}$) symmetry [24] with balanced gain and loss [25]. The loss and gain balance refers to the relationship between the total power dissipated by either the passive energy sinks in the structure itself (such as structural damping) or the power possibly absorbed by the active elements of the system [26], and the power injected into the system by the active elements of the system. Concern has been raised about whether globally lossless active systems can be engineered to the standard gain and phase margins that are traditionally required to ensure the stability and operational robustness of active control systems in practice [27]. For illustration, a large amount of recent work on the feedback approach to the active control of sound and vibration uses elaborated control strategies such as pole/zero placement techniques [28–30] or dedicated compensator circuits [31] to achieve so-called hyperstability [32].

A lumped parameter, active mechanical network exhibiting loss of reciprocity in terms of vibration transmission has been proposed in [33]. A feedback control system is used in which the control force is driven by a relative displacement signal amplified by a feedback gain. In the wave propagation direction of left-to-right, the control force depends on the error between the current cell and the previous cell. However in the wave propagation direction from right to left, the active control force depends on the error between the current cell and the next cell. In such a way, the spatial symmetry of the control force is broken by the asymmetric feedback signal. Simulation results assuming idealised transducers,

in particular a single component ("skyhook") control force, suggest a different displacement transmittance of the entire system for two opposite directions in a broad frequency band.

In contrast to the feedback approach described in [33], Tan et. al. [12] proposed a feedforward control strategy to achieve either unidirectional transmission or unidirectional absorption of sound in a one-dimensional waveguide. The former strategy employs a single monopole control source that is driven to minimise the transmitted wave, whereas the latter approach uses two monopole control sources that are driven to minimise both the reflected and transmitted waves and thus maximise the absorption. In both cases, a leaky filtered-reference least mean squares (FxLMS) adaptive algorithm [34] was used for the controller to converge to the optimal control source driving signals. The simulation results obtained suggest nearly perfect unidirectional sound transmission or absorption in the frequency band between 400 Hz and 1600 Hz.

The work reported in this paper builds on a recent notion [10] that a non-collocated sensor-actuator arrangement can be used within a model-free feedback approach to the active vibration control scheme to induce nonreciprocal vibration transmission. It should be noted that normally a collocated transducer arrangement is used to achieve stable and robust model-free feedback control systems [35]. If a non-collocated transducer arrangement is used, then the stability of the closed-loop system is not "automatically" guaranteed. However, it has been shown theoretically in [10] that stability properties similar to those of collocated transducer systems can still be accomplished, with the caveat that the passive structure under control falls into the family of so-called supercritical systems [36]. For example, if a simple two degree of freedom (DOF) active vibration isolation problem is considered, then it is necessary to ensure that the uncoupled natural frequency of the receiving body is lower than the uncoupled natural frequency of the source body [36]. Then, the potentially destabilising effects due to the non-collocated control force component can be successfully mitigated.

In [10], the loss of reciprocity based on a non-collocated sensor-actuator arrangement within a feedback control scheme was anticipated only theoretically. The potentially intricate dynamics of the non-ideal sensor-actuator transducers and their influence on the stability and performance properties of the control scheme were neglected. Moreover, a flexible active structure, characterised by an infinite number of vibration modes and natural frequencies, was just considered in a general demonstration that the reciprocity does not hold if the system is made active. Stability of the active system was only demonstrated for a particular (i.e. supercritical) family of 2DOF lumped parameter systems.

In this paper, the anticipations presented in [10] are verified theoretically and validated experimentally on a multiple DOF system. Considering the theoretical verification, an elaborate model of a 4DOF lumped parameter system equipped with two concurrent velocity feedback loops with non-collocated sensor-actuator pairs is derived. The model takes into account the dynamics of seismic accelerometers and electrodynamic force actuators. The experimental validation is carried out using a

3D-printed distributed parameter structure with embedded sensors and actuators. Both the theoretical and the experimental results show that, even though unconditional stability cannot be guaranteed, very large feedback gains can still be implemented. As a result, significant control effects and consequently a large broadband loss of reciprocity can be achieved. This implies the possibility of the practical implementation of the control scheme at hand in prospective active acoustic metamaterials for nonreciprocal sound transmission. The concept proposed has minimum stability and consequently minimum performance problems that normally stem from a non-collocated transducer arrangement [37]. Furthermore, stability and control performance problems that may arise from using a model-free MIMO control system without a centralised controller are circumvented by the careful design of the passive cell. This greatly simplifies the practical implementation by opening the way to use a model-free decentralised MIMO control system.

The paper is structured in five sections. In Section 2, the concept of the active metamaterial cell is introduced. In Section 3, two lumped parameter theoretical models, one neglecting and one including the transducer dynamics, are developed. The two models are used to carry out stability and control performance analyses. Section 4 is devoted to the experimental study and is followed by overall conclusions.

## 2 The active metamaterial cell concept

The concept of the active metamaterial cell is shown schematically in Figure 1. It is envisaged as a unit building block of a larger active sound barrier that consists of many such individual cells with an identical structure, as shown in Figure 2. Each cell consists of two pairs of panels $P_1$ and $P_2$ separated by a cavity $C_{2,1}$, which is filled with air in a pipe of a rectangular cross-section. It is assumed that the lateral walls of the rectangular pipe are rigid. In cavities $C_{1,2}$ between panels $P_1$ and $P_2$, which are also filled with air, there is an embedded force actuator which generates the control force by reacting off the panel $P_1$. The control force is proportional to the velocity of panel $P_2$ measured at the actuator footprint.

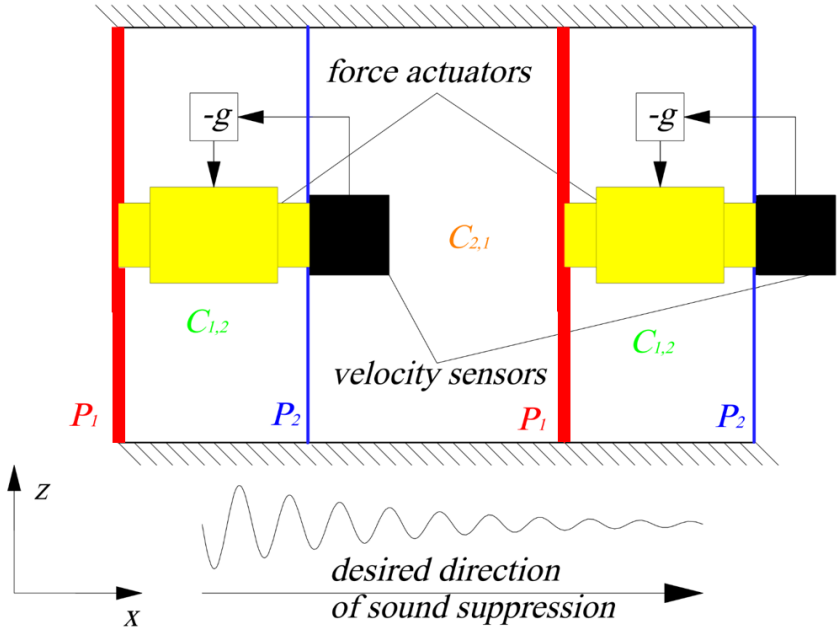


**Figure 1 Concept of the active acoustic metamaterial cell**

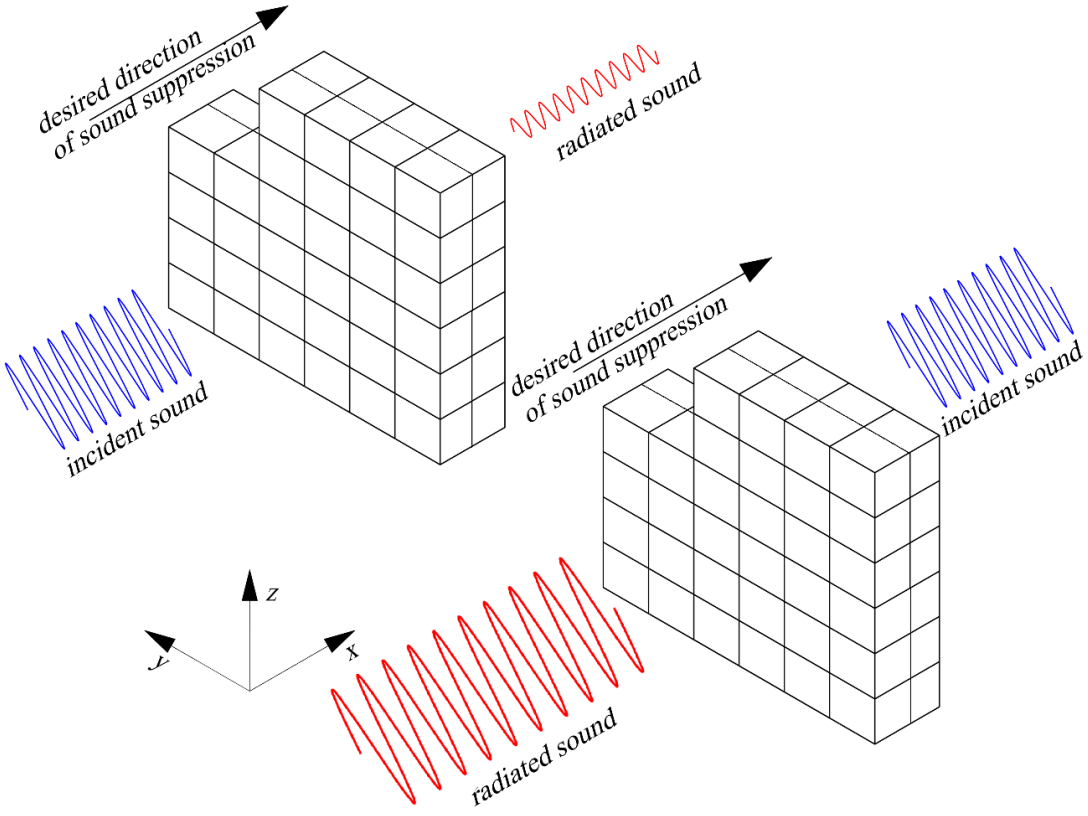


**Figure 2 Concept of the active acoustic metamaterial barrier**

Such a system may be modelled through a physics-based reduced-order model shown in Figure 4. The reduced-order model is formulated by considering only the fundamental, out-of-plane vibration mode (1,1) of panels $P_1$ and $P_2$ and the fundamental breathing modes (0,0,0) of air cavities $C_{1,2}$ and $C_{2,1}$. In such a reduced-order model, each panel is represented by a mass attached to a fixed reference base by a spring, and each cavity is represented by a spring connecting the masses representing the panels. The stiffness and masses in the lumped parameter reduced-order model depend on the dimensions, material properties and the boundary conditions of the four flexible panels and the dimensions of the three rectangular air cavities. A procedure for mapping the flexible panel/cavity properties to the discrete reduced-order model parameters, similar to that described in [38], may be used. This type of modelling neglects the higher-order coupled modes of the flexible quadruple panel configuration shown in Figure 1. Therefore, some of the global dynamic behaviour of the active system is lost for the benefit of a simpler and physically more transparent analysis.

# 3 Theoretical analysis of the active metamaterial cell

This section deals with the development and utilisation of two lumped parameter mathematical models of the active metamaterial cell. The first model considers the active system wherein the dynamic behaviour of the sensors and actuators is neglected. The second model is more elaborate, as it includes these initially neglected transducer dynamics. It is expected to provide a more realistic representation of the actual physical system considered in the experimental study given in Section 4.

## 3.1 Collocated versus non-collocated active vibration control

When considering feedback active vibration control, the location of and information flow within the sensor-actuator pairs has a great impact on the response of the closed-loop system. Collocation of sensors and actuators is best described graphically, using a 2DOF vibration system as an example, as indicated in Figure 3.

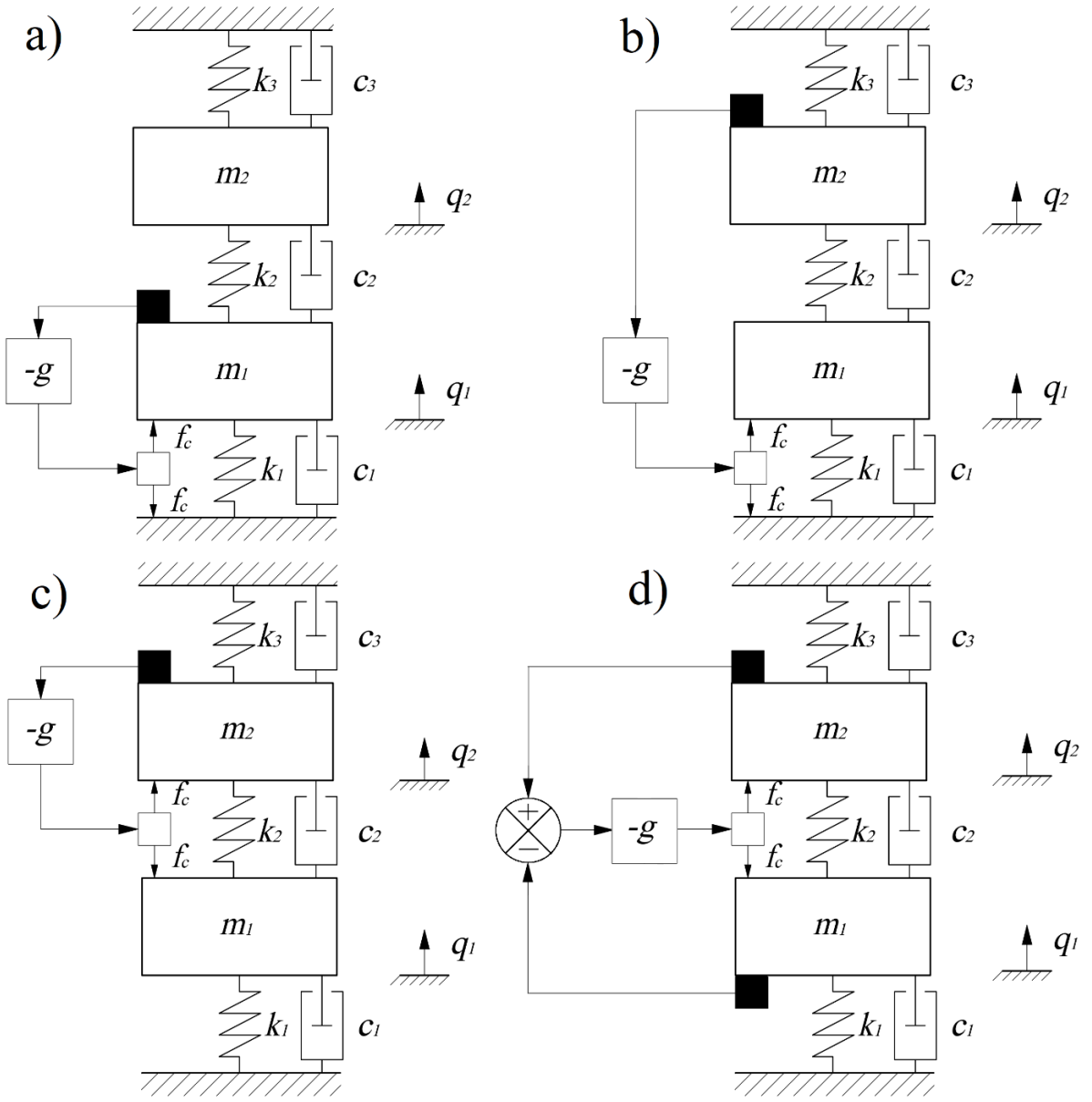


**Figure 3 Different configurations of sensors and actuators in active vibration control: a) collocated sensor-actuator pair, b) non-collocated sensor-actuator pair, c) non-collocated sensor-actuator pair, d) collocated sensor-actuator pair**

In Figure 3, sensors are represented by black and actuators by white squares. A sensor and an actuator are collocated if the actuator exerts a force $f_c$ on a degree of freedom whose kinematic variables are measured by the sensor (it is irrelevant whether displacement, velocity or acceleration is measured by the sensor). The influence of the collocation of sensors and actuators on the system's response can be investigated by considering the mass (if the sensors measure acceleration), damping (if the sensors measure velocity) or stiffness (if the sensors measure displacement) matrices of the system, provided that the transducers are ideal. In the present study, velocity feedback is considered (feedback gain $g$ has the same units as damping $c_1, c_2$ and $c_3$), so Table 1 shows the structure of the damping matrices of the various sensor-actuator configurations shown in Figure 3.

**Table 1 Damping matrices including passive damping and feedback gain for various sensor-actuator configurations in Figure 3**

| Sensor-actuator configuration | Damping matrix including passive damping and feedback gain |
|---|---|
| a) | $\begin{bmatrix} c_1 + c_2 + g & -c_2 \\ -c_2 & c_2 + c_3 \end{bmatrix}$ |
| b) | $\begin{bmatrix} c_1 + c_2 & -c_2 + g \\ -c_2 & c_2 + c_3 \end{bmatrix}$ |
| c) | $\begin{bmatrix} c_1 + c_2 & -c_2 - g \\ -c_2 & c_2 + c_3 + g \end{bmatrix}$ |
| d) | $\begin{bmatrix} c_1 + c_2 + g & -c_2 - g \\ -c_2 - g & c_2 + c_3 + g \end{bmatrix}$ |

The reciprocal behaviour of LTI systems is tied to their transfer function matrices and, for mechanical networks like the ones shown in Figure 3, these depend on the mass, damping and stiffness matrices. In particular, a system exhibits reciprocal behaviour if its transfer function matrix is symmetric. It can be shown that passive linear mechanical networks will satisfy this property, since their mass, stiffness and damping matrices are all symmetric. On the other hand, by introducing non-collocated control (sensor-actuator configurations b) and c) shown in Figure 3), at least one of the system matrices becomes diagonally asymmetric (in the example, the damping matrix) and the symmetry of the system's transfer function matrix is lost. For this reason, non-collocated control is chosen as a means of achieving nonreciprocal behaviour in the present study.

However, it should be mentioned that collocated control techniques are normally used to ensure good stability properties of the control system. In particular, the phase of the open-loop sensor-actuator FRF in a collocated control arrangement is confined to a 180 degree range since its amplitude is characterised by a resonance-antiresonance pattern in which, between each two resonances, an antiresonance can be found. Therefore, the control system stability using non-collocated transducer pairs requires special attention. Due to the fact that the two feedback loops operate concurrently (see Figure 1), they effectively form a decentralised Multi-Input-Multi-Output (MIMO) control system. This may cause further stability and performance problems due to the cross-talk between distant transducers, which could destabilise the whole system [37]. Therefore, as discussed in more detail in Section 3.6, a MIMO-stability analysis is needed.

## 3.2 Lumped parameter model of a single cell neglecting the transducer dynamics

The lumped parameter model of a single metamaterial cell is shown schematically in Figure 4. It consists of two identical 2DOF vibration subsystems with masses $m_1$ and $m_2$, stiffnesses $k_1, k_{1,2}, k_2$

and damping $c$ connected in series. Vibration transmission between the subsystems is facilitated by the coupling stiffness $k_{2,1}$. The components of the active system include velocity sensors mounted to degrees of freedom with mass $m_2$ and the reactive force actuators producing reactive control forces $f_{c1}$ and $f_{c2}$. These are made proportional to the measured velocities via proportionality constant (feedback gain) $g$. It should be noted that each of the sensor-actuator pairs is in a non-collocated configuration, since the force actuator uses one of the degrees of freedom, namely the one with mass $m_1$, as a base off which it reacts, without access to the velocity information of the corresponding degree of freedom. The entire control system is decentralised, since each of the individual controllers has access only to part of the system's state, and no information is exchanged between them. It is assumed for simplicity that the feedback gains of the two feedback loops are equal.

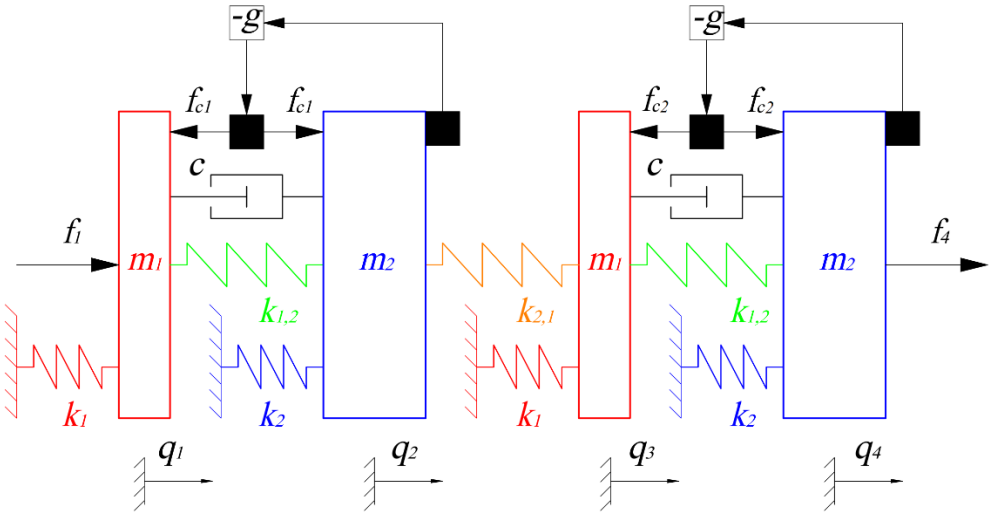


**Figure 4 Lumped parameter model of the metamaterial cell**

The equations of motion of the passive system are given as

$$\mathbf{M\ddot{q}} + \mathbf{D\dot{q}} + \mathbf{Kq} = \mathbf{f}, \tag{1a}$$

where **q** is the displacements vector

$$\mathbf{q}(t)^{\mathbf{T}} = [q_1(t) \quad q_2(t) \quad q_3(t) \quad q_4(t)], \tag{1b}$$

**F** is the vector of the external forces acting upon the degrees of freedom (in Figure 4, for clarity, only forces $f_1$ and $f_4$ are shown)

$$\mathbf{f}(t)^{\mathbf{T}} = [f_1(t) \quad f_2(t) \quad f_3(t) \quad f_4(t)], \tag{1c}$$

**M** is the mass matrix

$$\mathbf{M} = \begin{bmatrix} m_1 & 0 & 0 & 0 \\ 0 & m_2 & 0 & 0 \\ 0 & 0 & m_1 & 0 \\ 0 & 0 & 0 & m_2 \end{bmatrix}, \tag{1d}$$

**K** the stiffness matrix

$$\mathbf{K} = \begin{bmatrix} k_1 + k_{1,2} & -k_{1,2} & 0 & 0 \\ -k_{1,2} & k_{1,2} + k_2 + k_{2,1} & -k_{2,1} & 0 \\ 0 & -k_{2,1} & k_1 + k_{1,2} + k_{2,1} & -k_{1,2} \\ 0 & 0 & -k_{1,2} & k_{1,2} + k_2 \end{bmatrix}, \tag{1e}$$

and **D** is the damping matrix

$$\mathbf{D} = \begin{bmatrix} c & -c & 0 & 0 \\ -c & c & 0 & 0 \\ 0 & 0 & c & -c \\ 0 & 0 & -c & c \end{bmatrix}. \tag{1f}$$

It should be noted that damping is modelled through equal viscous dampers. Their terminals are attached only between the first and second and between the third and fourth mass. This is because this damping is a consequence of the air being pushed through the annular orifice of the miniature electrodynamic actuator which is used in each of the two feedback loops. This damping effect was found to be significantly more important than the structural damping of the rest of the system, which is thus assumed negligible.

For convenience of the analyses that follow, Eq. (1$a$) is reformulated into state space:

$$\dot{\mathbf{x}} = \mathbf{A}\mathbf{x} + \mathbf{B}\mathbf{u}, \tag{2a}$$

where **x** is the state vector composed of the system displacements and velocities

$$\mathbf{x}^{\mathbf{T}} = [\mathbf{q}^{\mathbf{T}} \quad \dot{\mathbf{q}}^{\mathbf{T}}], \tag{2b}$$

**u** is the input vector which is equal to the external forces applied to the system

$$\mathbf{u} = \mathbf{f}, \tag{2c}$$

while **A** and **B** are the state and the input matrices respectively:

$$\mathbf{A} = \begin{bmatrix} \mathbf{0} & \mathbf{I} \\ -\mathbf{M}^{-1}\mathbf{K} & -\mathbf{M}^{-1}\mathbf{D} \end{bmatrix}, \tag{2d}$$

$$\mathbf{B} = \begin{bmatrix} \mathbf{0} \\ \mathbf{M}^{-1} \end{bmatrix}, \tag{2e}$$

where **0** and **I** denote the 4×4 zero and identity matrices. Additionally, it is assumed that only the velocities of the system are measured, so the output equations are given as

$$\mathbf{y} = \mathbf{C}\mathbf{x}, \tag{3a}$$

where $\mathbf{y}$ is the output vector containing the velocities of the system

$$\mathbf{y} = \dot{\mathbf{q}}, \tag{3b}$$

and $\mathbf{C}$ is the output matrix, which is given as

$$\mathbf{C} = [\mathbf{0} \quad \mathbf{I}]. \tag{3c}$$

By taking the Laplace transform of Eqs. (2*a*) and (3*a*), the mapping from the input of the system to its output can be recovered:

$$\mathbf{Y}(s) = \mathbf{G_p}(s)\mathbf{U}(s), \tag{4a}$$

where $\mathbf{G_p}(s)$ is the transfer function matrix (mobility matrix) of the passive system given by Eq. (3*b*), $\mathbf{Y}(s)$ and $\mathbf{U}(s)$ are the Laplace transforms of the output and input vectors $\mathbf{y}(t)$ and $\mathbf{u}(t)$, whereas $s$ denotes the Laplace variable:

$$\mathbf{G_p}(s) = \mathbf{C}(s\mathbf{I} - \mathbf{A})^{-1}\mathbf{B}. \tag{4b}$$

The transfer function matrix $\mathbf{G_p}(s)$ is symmetric, which indicates the reciprocal behaviour of the passive system. Physically, this means that the system transmits vibrations in its two characteristic directions (left to right and right to left – see Figure 4) equally. Active control is introduced according to the block diagram in Figure 5. The output $\mathbf{Y}$ is measured by means of the velocity sensors, which are denoted by the matrix $\mathbf{G_s}$. This measured signal is then fed to the proportional controller $\mathbf{G_c}$ to generate control forces $\mathbf{F_c}$ (see Figure 4).

It is assumed at this stage that both the sensors and the actuators are ideal. This is modelled through matrices $\mathbf{G_s}$ and $\mathbf{G_c}$, which are of the following structure:

$$\mathbf{G_s} = \begin{bmatrix} 0 & 1 & 0 & 0 \\ 0 & 0 & 0 & 1 \end{bmatrix}, \tag{5a}$$

$$\mathbf{G_c} = \begin{bmatrix} -g & 0 \\ g & 0 \\ 0 & -g \\ 0 & g \end{bmatrix}. \tag{5b}$$

According to Eq. (5*a*), the system velocities are directly mapped to the error velocities required for control, $\mathbf{Y}(s)$, since matrix $\mathbf{G_s}$ is populated with ones and zeros only. On the other hand, these error velocities are mapped to the control forces $\mathbf{F_c}$ via the controller matrix $\mathbf{G_c}$. Since its elements (the feedback gains $g$) all have the dimension $\mathrm{Nsm^{-1}}$, they may be considered to deliver a sort of "active damping" to masses $m_2$ with a collocated error velocity sensor. However, the reactive component of the

control force could both extract and inject energy at masses $m_1$. In other words, it cannot be guaranteed that the reactive control force component strictly absorbs energy.

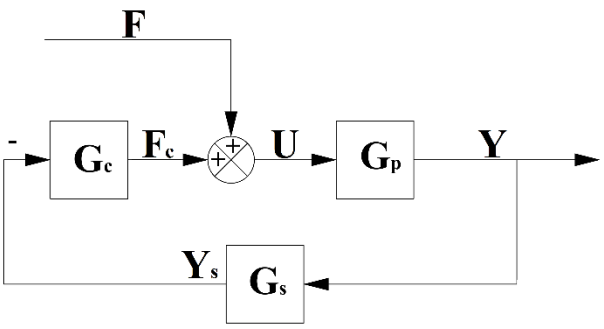


**Figure 5 Block diagram of the active metamaterial cell**

Following the rules of block algebra, one can obtain the mapping from the external inputs to the system, $\mathbf{F}(s)$, to the output velocities $\mathbf{Y}(s)$:

$$\mathbf{Y}(s) = \mathbf{G}(s)\mathbf{F}(s), \tag{6a}$$

where the transfer function matrix of the active system $\mathbf{G}(s)$ is given by:

$$\mathbf{G}(s) = \left[\mathbf{I} + \mathbf{G_p}(s)\mathbf{G_c}\mathbf{G_s}\right]^{-1}\mathbf{G_p}(s). \tag{6b}$$

By analysing the structure of Eq. (6*b*), it can be shown that matrix $\mathbf{G}$ is not symmetric when control is switched on (i.e. when $g \neq 0$), and thus the system does not exhibit reciprocity. An example is given at the end of the following subsection.

Since such an active system implements two decentralised velocity feedback loops, in which the sensors and actuators are not collocated, a detailed stability analysis is required to determine how to design the passive system before control is implemented so that the active system with control remains stable for all positive feedback gains $g$.

### 3.3 Stability

In order to carry out the stability analysis, the Routh-Hurwitz stability criterion is used. In order to apply the Routh-Hurwitz criterion, it is necessary to analyse the characteristic polynomial of a closed-loop system. A closed-loop active system is stable if all roots of its characteristic polynomial have negative real parts. This stability criterion is convenient because it enables one to determine if an active system has a pole with a positive real part without calculating the roots of a potentially high order polynomial [39]. In the present study, the characteristic polynomial can be calculated as the denominator of any of the 16 transfer functions contained in the matrix $\mathbf{G}(s)$ given by Eq. (6*b*). Each of these transfer functions is given by:

$$G_{i,j}(s) = \frac{N_{i,j}(s)}{D(s)}, \tag{7}$$

where $N_{i,j}(s)$ denotes the numerator and $D(s)$ the denominator of the transfer function. Both functions are polynomials in $s$. Since $D(s)$ is polynomial of order eight and as such in general its roots cannot be determined analytically, the Routh-Hurwitz criterion becomes especially useful.

At this point in the analysis it is useful to introduce dimensionless parameters in order to generalise the stability analysis to the family of all systems that follow the layout shown in Figure 4. To this end, the following dimensionless parameters are introduced:

$$\text{dimensionless Laplace variable: } \tilde{s} = \frac{s}{\Omega_1}, \tag{8a}$$

circular frequency ratios:

$$\alpha = \left(\frac{\Omega_2}{\Omega_1}\right)^2, \tag{8b}$$

$$\beta = \left(\frac{\Omega_3}{\Omega_1}\right)^2, \tag{8c}$$

$$\gamma = \left(\frac{\Omega_4}{\Omega_1}\right)^2, \tag{8d}$$

$$\text{dimensionless damping: } \zeta = \frac{c}{2\sqrt{k_1 m_1}}, \tag{8e}$$

$$\text{mass ratio: } \mu = \frac{m_2}{m_1}, \tag{8f}$$

$$\text{dimensionless feedback gain: } \eta = \frac{g}{c}, \tag{8g}$$

where $\Omega_1, \Omega_2, \Omega_3$ and $\Omega_4$ represent derived circular frequencies defined by the following expressions:

$$\Omega_1 = \sqrt{\frac{k_1}{m_1}}, \tag{8h}$$

$$\Omega_2 = \sqrt{\frac{k_{1,2}}{m_2}}, \tag{8i}$$

$$\Omega_3 = \sqrt{\frac{k_2}{m_2}}, \tag{8j}$$

$$\Omega_4 = \sqrt{\frac{k_{2,1}}{m_2}}. \tag{8k}$$

Although it was mentioned that the denominator in Eq. (7) is a polynomial of order eight, its structure allows for a factorisation into two polynomials of order four:

$$D(\tilde{s}) = \sqrt{k_1 m_1} P_1^{(4)}(\tilde{s}) P_2^{(4)}(\tilde{s}), \tag{9}$$

where polynomials $P_1^{(4)}(\tilde{s})$ and $P_2^{(4)}(\tilde{s})$ are given by the expressions that follow:

$$\begin{gathered} P_1^{(4)}(\tilde{s}) = \mu\tilde{s}^4 + 2\zeta(1+\eta+\mu)\tilde{s}^3 + \mu(1+\alpha+\beta+\mu\alpha)\tilde{s}^2 + \\ +2\zeta(1+\beta\mu+\eta)\tilde{s} + \mu(\mu\beta\alpha+\beta+\alpha), \end{gathered} \tag{10a}$$

$$\begin{gathered} P_2^{(4)}(\tilde{s}) = \mu\tilde{s}^4 + 2\zeta(\mu+1+\eta)\tilde{s}^3 + \mu(1+\alpha+\beta+\gamma+\mu\alpha+\mu\gamma)\tilde{s}^2 + \\ +2\zeta(1+\eta+\mu\beta+2\mu\gamma+\mu\gamma\eta)\tilde{s} + \\ +\mu^2[\alpha\beta+\gamma(2\alpha+\beta)] + \mu(\alpha+\beta+\gamma). \end{gathered} \tag{10b}$$

This possibility for factorisation stems from the repetitive geometry of the unit cell considered, i.e. the 4 dof system is obtained by connecting two identical 2 dof systems in series.

In order to ensure the negativity of the real parts of the roots of the denominator defined by Eq. (9), both polynomials defined by Eqs. (10*a*) and (10*b*) must simultaneously have negative real parts of their roots. Here, discussion of the stability of two fourth-order systems is a simpler task than the corresponding task for the eighth-order system.

The necessary stability condition states that a polynomial has roots with negative real parts if all of its coefficients have the same sign. This may be straightforwardly shown for the polynomials defined by Eqs. (10*a*) and (10*b*), since all of the dimensionless parameters of the system are positive by definition. However, this condition is not sufficient to prove stability, which is why an analysis of the Hurwitz determinants of the polynomials defined by Eqs. (10*a*) and (10*b*) is conducted next ($\Delta_{i,j}$ denotes the *i*-th Hurwitz determinant of the *j*-th polynomial):

$$\Delta_{1,1} = 2\zeta(\eta+\mu\beta+1), \tag{11a}$$

$$\Delta_{2,1} = 2\mu\zeta\{1+\eta+\mu[\alpha\eta(1-\beta)+\beta^2]\}, \tag{11b}$$

$$\Delta_{3,1} = 4\zeta^2\mu^2(1-\beta)\{\alpha\eta^2+1-\beta+\eta[1-\beta+\alpha(1+\mu)]\}, \tag{11c}$$

$$\Delta_{4,1} = 4\zeta^2\mu^3(1-\beta)\{\alpha\eta^2+1-\beta+\eta[1-\beta+\alpha(1+\mu)]\}, \tag{11d}$$

$$\Delta_{1,2} = 2\zeta\{1+\eta+\mu[\beta+\gamma(2+\eta)]\}, \tag{12a}$$

$$\Delta_{2,2} = 2\mu\zeta\left\{\begin{gathered}1+\eta+\mu[\alpha\eta(1-\beta)+\beta^2+\gamma^2(2+\eta)+\gamma(2+2\beta+2\eta)]+\\ +\gamma^2\mu^2(2+\eta)+\mu\gamma\alpha\eta(\mu-1)\end{gathered}\right\}, \tag{12b}$$

$$\Delta_{3,2} = 4\mu^2\zeta^2\left\{\begin{gathered}\eta^2[\gamma^2+\alpha\gamma(\mu-1)+\alpha(1-\beta)]+\\ +\eta\left[\begin{gathered}\gamma^2(3+\mu^2)+\gamma(\mu-1)(\mu\alpha+2(1-\beta)+\alpha)+\\ +(1-\beta)(1-\beta+\alpha+\mu\alpha)\end{gathered}\right]+\\ +\gamma^2(2+2\mu^2)+2\gamma(1-\beta)(\mu-1)+(\beta-1)^2\end{gathered}\right\}, \tag{12c}$$

$$\Delta_{4,2}= 4\mu^3\zeta^2 \left\{ \begin{array}{c} \eta^2[\gamma^2 + \alpha\gamma(\mu-1) + \alpha(1-\beta)] + \\ +\eta\left[\begin{array}{c}\gamma^2(3+\mu^2) + \gamma(\mu-1)(\mu\alpha + 2(1-\beta) + \alpha) + \\ +(1-\beta)(1-\beta+\alpha+\mu\alpha)\end{array}\right] + \\ \gamma^2(2+2\mu^2) + 2\gamma(1-\beta)(\mu-1) + (\beta-1)^2 \end{array} \right\}. \qquad (12d)$$

In order for the active system to be stable, the positivity of each of these determinants must be ensured for all nonnegative values of the dimensionless feedback gain $\eta$. By considering each element in the previous determinants where subtraction occurs, one can conclude that the active system is stable for all $\eta \geq 0$ if:

$$\beta < 1 \rightarrow \sqrt{\frac{k_2}{m_2}} < \sqrt{\frac{k_1}{m_1}}, \text{and} \qquad (13)$$

$$\mu > 1 \rightarrow m_2 > m_1. \qquad (14)$$

Condition (14) is merely a requirement for masses $m_2$ (denoted in blue in Figure 4) to be larger than masses $m_1$ (denoted in red in Figure 4). On the other hand, condition (13) is analogous to the inequality derived in [36] for a two degree of freedom system equipped with a similar active control system.

The influence of inequalities (13) and (14) on the stability properties of the system may be visualised by plotting the Hurwitz determinants, defined by Eqs. (11) and (12), as functions of the dimensionless feedback gain $\eta$. Figure 6 represents the case where conditions (13) and (14) are satisfied and the system is unconditionally stable, i.e. all Hurwitz determinants are positive for all $\eta \geq 0$. However, if conditions (13) and (14) are not met, then the Hurwitz determinants assume shapes as shown in Figure 7, where it is clear that there exists only a finite interval of the dimensionless feedback gain $\eta$ for which the system is stable.

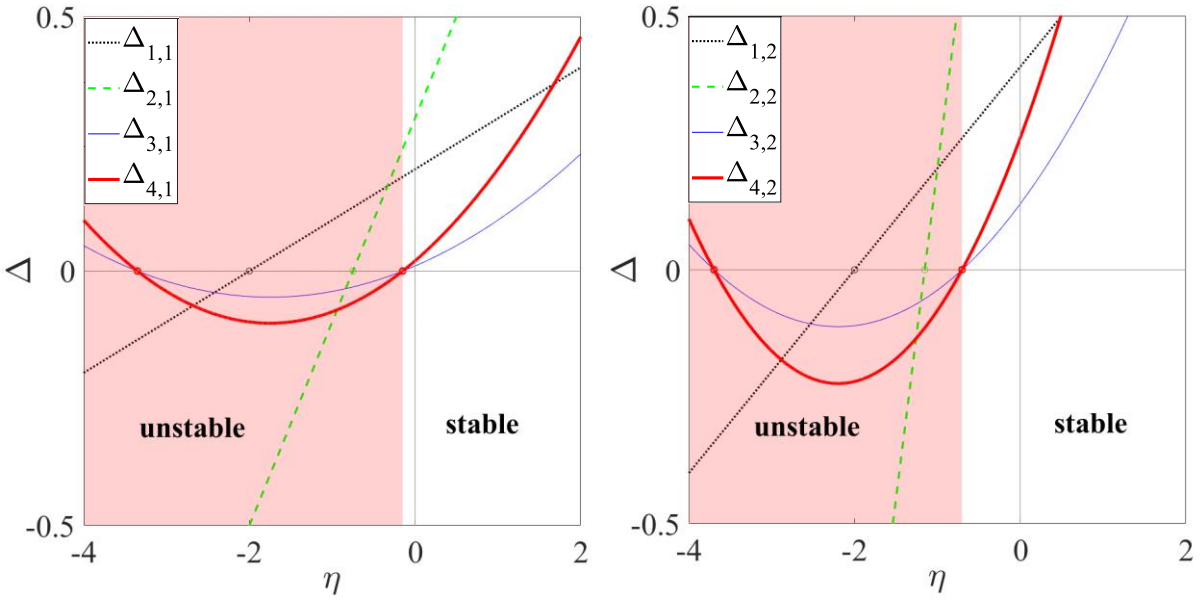


**Figure 6 Hurwitz determinants for the case of an unconditionally stable active system with parameters:**

$$\boldsymbol{\alpha = 1, \beta = \frac{1}{2}, \gamma = \frac{1}{2}, \mu = 2, \zeta = \frac{1}{20}}$$

**($\Delta_{1,j}$ – dotted black line, $\Delta_{2,j}$ – dashed green line, $\Delta_{3,j}$ – faint blue line, $\Delta_{4,j}$ – thick red line)**

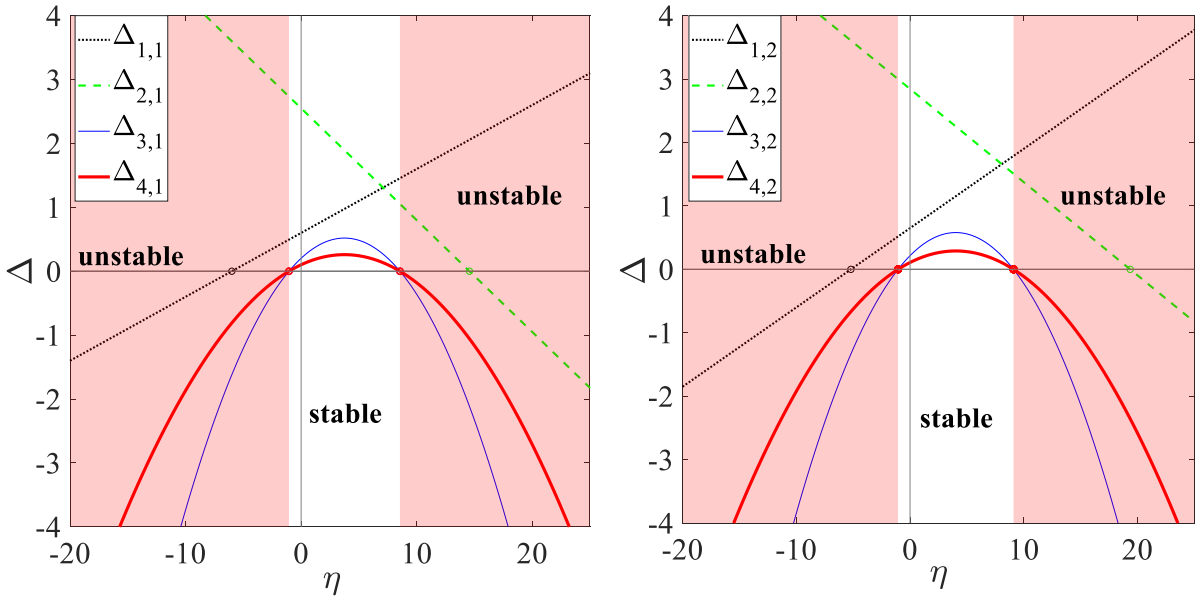


**Figure 7 Hurwitz determinants for the case of a conditionally stable active system with parameters:**

$$\boldsymbol{\alpha = 1, \beta = 10, \gamma = \frac{1}{2}, \mu = \frac{1}{2}, \zeta = \frac{1}{20}}$$

**($\Delta_{1,j}$ – dotted black line, $\Delta_{2,j}$ – dashed green line, $\Delta_{3,j}$ – faint blue line, $\Delta_{4,j}$ – thick red line)**

The expressions for transfer mobilities $G_{1,4}(\tilde{s})$ and $G_{4,1}(\tilde{s})$ are given as follows:

$$G_{1,4}(\tilde{s}) = \frac{\mu\gamma\tilde{s}(2\zeta(\eta+1)\tilde{s} + \mu\alpha)^2}{D(\tilde{s})}, \tag{15a}$$

$$G_{4,1}(\tilde{s}) = \frac{\mu\gamma\tilde{s}(2\zeta\tilde{s} + \mu\alpha)^2}{D(\tilde{s})}. \tag{15b}$$

These functions quantify the transmission of vibration from right to left, $G_{1,4}(\tilde{s})$, and left to right, $G_{4,1}(\tilde{s})$, see Figure 4. They are not equal when $\eta \neq 0$ (i.e. when the system is active), and therefore the activated system does not comply with the reciprocity principle.

So far it has been shown that it is possible to determine the parameters of the passive system so that the active system is unconditionally stable. Therefore the next subsection deals with the performance of the active system, i.e. with the efficiency with which the active system induces the nonreciprocal effects in terms of the difference between the two transfer mobilities $G_{1,4}(\tilde{s})$ and $G_{4,1}(\tilde{s})$.

### 3.4 Performance

In order to assess the performance of the active metamaterial cell, the $\mathcal{H}_2$ norm of transfer mobilities $G_{1,4}(s)$ and $G_{4,1}(s)$ is used. In general, the $\mathcal{H}_2$ norm of transfer functions provides a valid metric for assessing performance of vibration control systems. Its square represents the variance of the output of the system, when the input is either white Gaussian noise or an ideal impact [40]. In addition, since velocity is chosen as the output variable, the square of the $\mathcal{H}_2$ norm is also proportional to the kinetic energy of the corresponding mass. Thus, the norm has an additional physical interpretation. In general, the square of the $\mathcal{H}_2$ norm of a single (scalar) stable transfer function $G_{k,l}(s)$ is given by the following integral:

$$\left\|G_{k,l}(\mathrm{j}\omega)\right\|_{\mathcal{H}_2}^2 = \frac{1}{2\pi}\int_{-\infty}^{\infty}\left|G_{k,l}(\mathrm{j}\omega)\right|^2 \mathrm{d}\omega, \tag{16}$$

where j is the imaginary unit, $\omega$ the angular frequency, and $k,l=1\ldots4$. The $\mathcal{H}_2$ norm of transfer mobilities $G_{1,4}$ and $G_{4,1}$ of the active system may be calculated as functions of the feedback gain $g$ in order to observe changes in vibration transmission as $g$ increases. As an example, the $\mathcal{H}_2$ norm is calculated with parameters of the passive mechanical system given in Table 2. These parameters have been chosen so that inequalities (13) and (14) are satisfied, in such a way that an arbitrarily large feedback gain $g$ may be applied without the system becoming unstable.

**Table 2 Lumped parameters of the metamaterial cell**

| parameter | value |
|---|---|
| $m_1$ | 0.005 kg |
| $m_2$ | 0.0075 kg |
| $k_1$ | 50000 N m$^{-1}$ |
| $k_2$ | 9000 N m$^{-1}$ |
| $k_{1,2}$ | 20000 N m$^{-1}$ |
| $k_{2,1}$ | 15000 N m$^{-1}$ |
| $c = c_{1,2}$ | 0.1 N s m$^{-1}$ |

Figure 8 shows the $\mathcal{H}_2$ norm of the characteristic transfer mobilities of the active system as a function of the feedback gain. In particular, the $\mathcal{H}_2$ norms in the figure are normalised with the $\mathcal{H}_2$ norms when the system is passive:

$$\left\|\tilde{G}_{1,4}\right\|_{\mathcal{H}_2} = \frac{\left\|G_{1,4}\right\|_{\mathcal{H}_2}}{\left\|G_{1,4}(g=0)\right\|_{\mathcal{H}_2}}, \tag{17a}$$

$$\left\|\tilde{G}_{4,1}\right\|_{\mathcal{H}_2} = \frac{\left\|G_{4,1}\right\|_{\mathcal{H}_2}}{\left\|G_{4,1}(g=0)\right\|_{\mathcal{H}_2}}. \tag{17b}$$

It is evident in Figure 8 that the active system transmits vibrations differently in the two directions. In particular, the $\mathcal{H}_2$ norm of transfer mobility $G_{4,1}(s)$ monotonically decreases when the feedback gain $g$ is increased. On the other hand, vibration transmission in the opposite direction decreases at first, due to the effect of damping down the resonant response, but with a further increase of the feedback gain $g$, the $\mathcal{H}_2$ norm of $G_{1,4}(s)$ starts to increase. In fact, for significantly large gains it becomes larger than in the case where the system is passive.

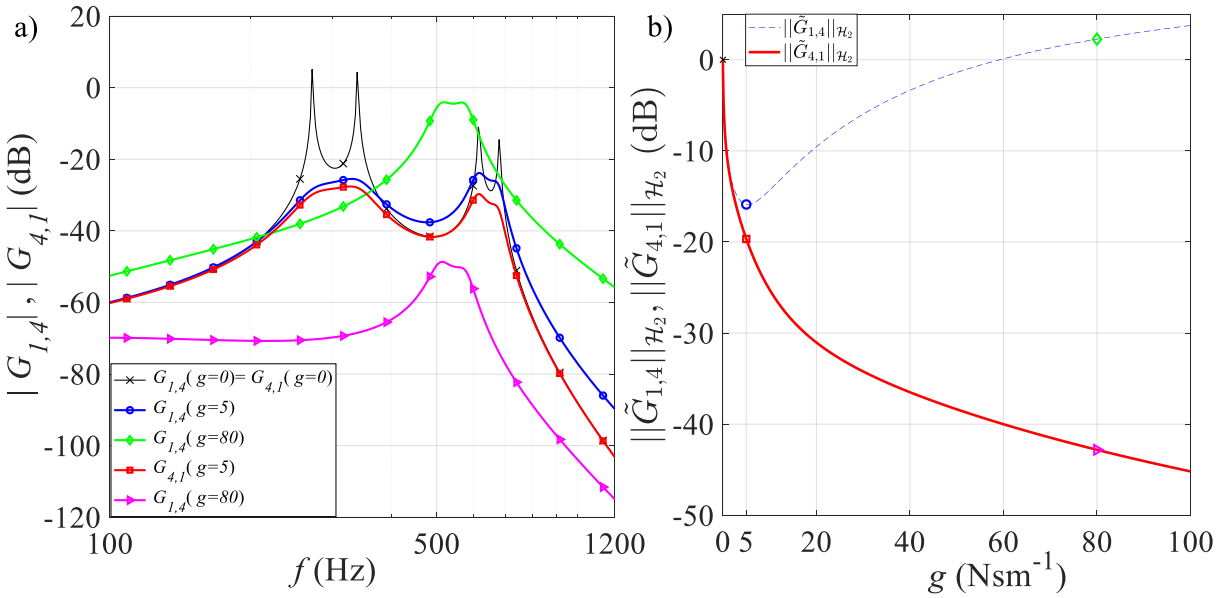


**Figure 8 Amplitudes of characteristic transfer mobilities with different feedback gains (a) and $\mathcal{H}_2$ norms of characteristic transfer mobilities (b)**

The theoretical considerations of this subsection give strong indications that the proposed active system may be used in practice to achieve a nonreciprocal response. Before the development of an experimental prototype which will be used to validate the theoretical findings, a more elaborate model of the system at hand is developed in the following subsection, taking into account the initially neglected sensor-actuator dynamics.

## 3.5 Lumped parameter model including sensor-actuator dynamics

The transducer dynamics are incorporated into the model, thereby fully coupling the mechanical and electrical subsystems. This in turn allows for a more faithful representation of the actual physical system. The scheme of this augmented model is given in Figure 9. The electrodynamic actuators are modelled as first-order electrical systems with resistance $R$, inductance $L$, and a back electromotive force constant $T$, which is equal in value (but different in units) to the force proportionality constant which relates the electrical current flowing through the circuit to the produced force. Since vibration transmission is monitored only from the leftmost degree of freedom to the rightmost and vice versa, only two driving actuators are used in the model, producing excitation forces $f_1$ and $f_4$ as a result of applied voltages $e_1$ and $e_4$.

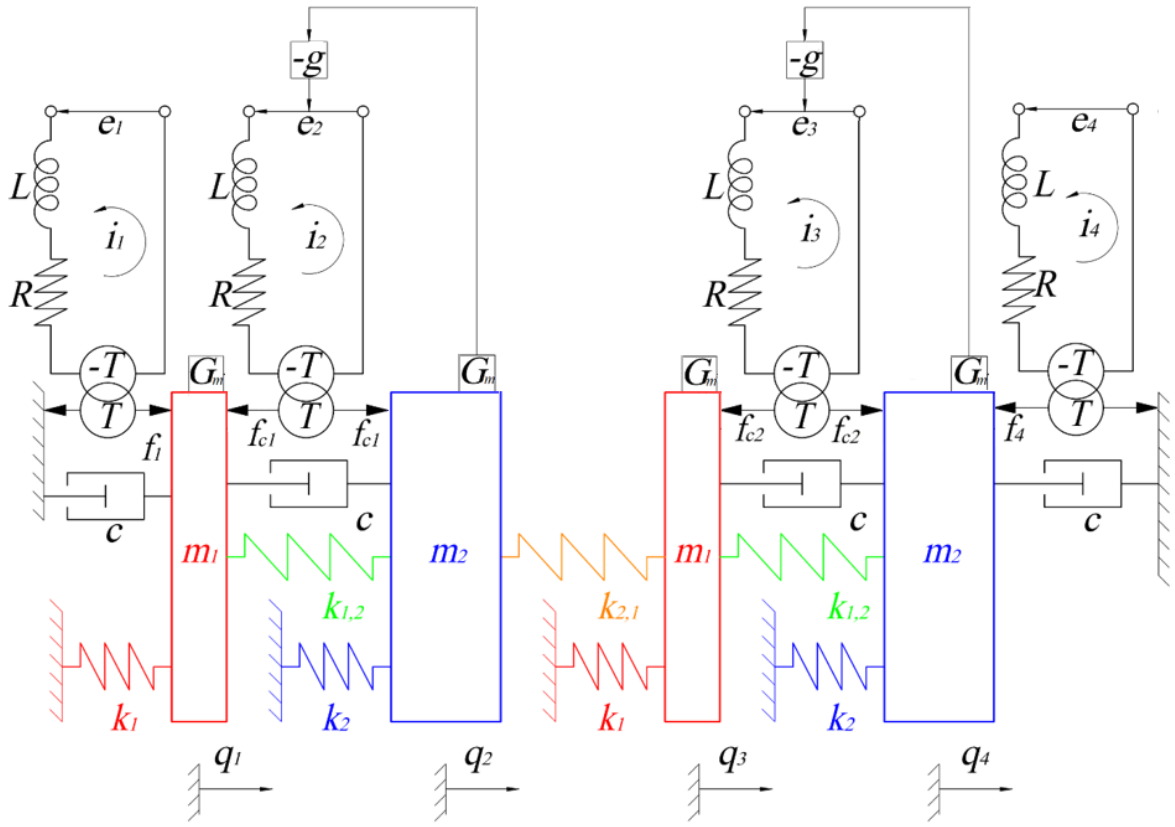


**Figure 9 Model of the active metamaterial cell including sensor-actuator dynamics**

Assuming that all actuators are identical, their dynamic behaviour may be written in matrix form:

$$\frac{\mathrm{d}\mathbf{i}}{\mathrm{d}t} = -\frac{R}{L}\mathbf{i} + \frac{T}{L}\mathbf{N}^{\mathbf{T}}\dot{\mathbf{q}} + \frac{1}{L}\mathbf{e}, \tag{18a}$$

where **i** is the vector containing the electrical currents passing through the actuator circuits:

$$\mathbf{i}^{\mathbf{T}} = [i_1 \quad i_2 \quad i_3 \quad i_4], \tag{18b}$$

**e** is the actuator voltage vector:

$$\mathbf{e}^{\mathbf{T}} = [e_1 \quad e_2 \quad e_3 \quad e_4], \tag{18c}$$

and matrix **N** is populated as follows:

$$\mathbf{N} = \begin{bmatrix} -1 & 1 & 0 & 0 \\ 0 & -1 & 0 & 0 \\ 0 & 0 & 1 & 0 \\ 0 & 0 & -1 & 1 \end{bmatrix}. \tag{18d}$$

As mentioned earlier, the forces which act upon the mechanical subsystem are proportional to the currents flowing through the electrical circuits:

$$\mathbf{f}^{\mathbf{T}} = [f_1 \quad f_{c1} \quad f_{c2} \quad f_4] = T\mathbf{i}^{\mathbf{T}}, \tag{18e}$$

so that the equations of motion of the mechanical subsystem may be written as the following equation:

$$\mathbf{M}\ddot{\mathbf{q}} + \mathbf{D}\dot{\mathbf{q}} + \mathbf{K}\mathbf{q} + T\mathbf{N}\mathbf{i} = \mathbf{0}, \tag{19a}$$

with matrices **M** and **K** being identical to the ones defined by Eqs. (1*d*) and (1*e*), but the damping matrix **D** is given by:

$$\mathbf{D} = \begin{bmatrix} 2c & -c & 0 & 0 \\ -c & c & 0 & 0 \\ 0 & 0 & c & -c \\ 0 & 0 & -c & 2c \end{bmatrix}. \tag{19b}$$

The structure of the damping matrix is different from Eq. (1*f*) since the excitation forces $f_1$ and $f_4$ are applied via electrodynamic actuators, which add passive air-gap damping as mentioned earlier in subsection 3.2.

Equations (18*a*) and (19*a*) may be written as a system of first-order ordinary differential equations. This yields a state space representation of the system:

$$\dot{\hat{\mathbf{x}}} = \hat{\mathbf{A}}\hat{\mathbf{x}} + \hat{\mathbf{B}}\hat{\mathbf{u}}, \tag{20a}$$

$$\hat{\mathbf{y}} = \hat{\mathbf{C}}\hat{\mathbf{x}}, \tag{20b}$$

where $\hat{\mathbf{x}}$ is the augmented state vector including both the mechanical states (displacements and velocities) as well as the electrical states (currents) of the corresponding subsystems:

$$\hat{\mathbf{x}}^{\mathbf{T}} = [\mathbf{q}^{\mathbf{T}} \quad \dot{\mathbf{q}}^{\mathbf{T}} \quad \mathbf{i}^{\mathbf{T}}], \tag{20c}$$

$\hat{\mathbf{u}}$ is the input vector containing the voltages imposed at the electrodynamic actuators' electrical terminals:

$$\hat{\mathbf{u}} = \mathbf{e}, \tag{20d}$$

while the outputs of the system remain the velocities of the four degrees of freedom, as in subsection 3.2:

$$\hat{\mathbf{y}} = \dot{\mathbf{q}}. \tag{20e}$$

The augmented system matrix is given as follows:

$$\hat{\mathbf{A}} = \begin{bmatrix} \mathbf{0} & \mathbf{I} & \mathbf{0} \\ -\mathbf{M}^{-1}\mathbf{K} & -\mathbf{M}^{-1}\mathbf{D} & -T\mathbf{M}^{-1}\mathbf{N} \\ \mathbf{0} & \frac{T}{L}\mathbf{N}^{\mathbf{T}} & -\frac{R}{L}\mathbf{I} \end{bmatrix}, \tag{20f}$$

where **I** and **0** are again 4×4 identity and null-matrices. By representing the system in such an augmented state space, the coupling between the mechanical and electrical subsystems can be clearly identified. In particular, the first 2×2 block of matrices in Eq. (20*f*) is identical to the matrix defined by Eq. (2*d*) and

shows how the mechanical states (displacements and velocities) influence one another. On the other hand, elements $-T\mathbf{M^{-1}N}$ and $\frac{T}{L}\mathbf{N^T}$ are related to how the electrical subsystem influences the mechanical one and vice versa.

The augmented input matrix $\widehat{\mathbf{B}}$ is defined as:

$$\widehat{\mathbf{B}} = \begin{bmatrix} \mathbf{0} \\ \mathbf{0} \\ 1 \\ \frac{1}{L}\mathbf{I} \end{bmatrix}, \tag{20g}$$

where $\mathbf{I}$ and $\mathbf{0}$ are again 4×4 identity and zero matrices.

Finally, the augmented output matrix $\widehat{\mathbf{C}}$ is given as follows:

$$\widehat{\mathbf{C}} = [\mathbf{0} \quad \mathbf{I} \quad \mathbf{0}], \tag{20h}$$

where $\mathbf{0}$ and $\mathbf{I}$ are zero and identity matrices with dimensions 4×4.

The transfer function matrix of the passive system augmented with actuator dynamics is defined as:

$$\widehat{\mathbf{G}}_\mathbf{p}(s) = \widehat{\mathbf{C}}\left(s\mathbf{I} - \widehat{\mathbf{A}}\right)^{-1}\widehat{\mathbf{B}}, \tag{21}$$

and represents the mapping of voltages at the electrical terminals of the electrodynamic actuators to the velocities of the mechanical degrees of freedom.

The application of the active control to the system is done according to the block diagram in Figure 10. This diagram is quite similar to the one in subsection 3.2. However, the matrices which represent the system elements are populated differently. The sensor matrix $\widehat{\mathbf{G}}_\mathbf{s}(s)$ is defined by:

$$\widehat{\mathbf{G}}_\mathbf{s}(s) = \mathrm{diag}[G_m(s), G_m(s), G_m(s), G_m(s)], \tag{22a}$$

$$G_m(s) = \frac{\omega_m^2}{\omega_m^2 + 2\zeta_m\omega_m s + s^2}, \tag{22b}$$

and its elements are second-order transfer functions defined by Eq. (22*b*). Second-order dynamics are used for sensor modelling since inertial accelerometers used to measure vibration responses normally contain seismic masses and act as 1DOF vibration systems themselves, having a relatively high natural frequency $\omega_m$ and a relatively low damping ratio $\zeta_m$. It is assumed in Eq. (22*b*) that the gain of the second-order system is absorbed in the feedback gain $\hat{g}$. Additionally, it is assumed that all sensors are identical.

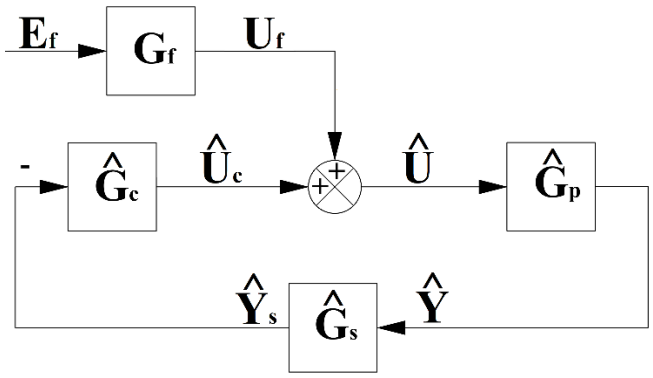


**Figure 10 Block diagram of the active metamaterial cell augmented with sensor-actuator dynamics**

The controller is given by the transfer function matrix $\hat{\mathbf{G}}_\mathbf{c}$, which represents the mapping from the measured velocities of the system $\hat{\mathbf{Y}}_\mathbf{s}(s)$ to the control voltages $\hat{\mathbf{U}}_\mathbf{c}(s)$. Note that the units of feedback gains $\hat{g}$ are now Vsm$^{-1}$ (since voltage is the control variable), as opposed to the case from previous subsections, where idealised actuators were assumed and the feedback gain $g$ had units Nsm$^{-1}$:

$$\hat{\mathbf{G}}_\mathbf{c} = \begin{bmatrix} 0 & 0 & 0 & 0 \\ 0 & \hat{g} & 0 & 0 \\ 0 & 0 & 0 & \hat{g} \\ 0 & 0 & 0 & 0 \end{bmatrix}. \tag{22c}$$

The zero-rows in matrix $\hat{\mathbf{G}}_\mathbf{c}$ are required to keep the dimensions of the control voltages consistent with the dimensions of the input vector, even though only voltages $e_2$ and $e_3$ are used for control. For the same reasons, matrix $\mathbf{G_f}$ is required and serves only to expand the vector of excitation voltages $\mathbf{E_f}(s)$ and recover the external excitation vector $\mathbf{U_f}(s)$:

$$\mathbf{E_f^T}(s) = [E_1(s) \quad E_4(s)], \tag{22d}$$

$$\mathbf{G_f} = \begin{bmatrix} 1 & 0 \\ 0 & 0 \\ 0 & 0 \\ 0 & 1 \end{bmatrix}, \tag{22e}$$

where $E_1(s)$ and $E_4(s)$ represent the Laplace transforms of voltages $e_1(t)$ and $e_4(t)$.

The mapping from the excitation voltages $\mathbf{E_f}(s)$ to the measured velocities $\hat{\mathbf{Y}}_\mathbf{s}(s)$ is given by:

$$\hat{\mathbf{Y}}_\mathbf{s}(s) = \hat{\mathbf{G}}(s)\mathbf{E_f}(s), \tag{23a}$$

$$\hat{\mathbf{G}}(s) = \left[\mathbf{I} + \hat{\mathbf{G}}_\mathbf{s}(s)\hat{\mathbf{G}}_\mathbf{p}(s)\hat{\mathbf{G}}_\mathbf{c}\right]^{-1}\hat{\mathbf{G}}_\mathbf{s}(s)\hat{\mathbf{G}}_\mathbf{p}(s)\mathbf{G_f}. \tag{23b}$$

The characteristic transfer functions analogous to the transfer mobilities $G_{1,4}$ and $G_{4,1}$ of the model neglected transducer dynamics become elements $\hat{G}_{1,2}$ and $\hat{G}_{4,1}$ of matrix $\hat{\mathbf{G}}(s)$. They represent the mapping of voltage $e_4$ to the measured velocity of the first degree of freedom and the mapping of voltage $e_1$ to the measured velocity of the fourth degree of freedom. Because of this, even though it does not

represent a mapping from forces to velocities (but rather voltages to velocities), matrix $\widehat{\mathbf{G}}(s)$ may be considered analogous to the mobility matrix of the active system $\mathbf{G}(s)$ when the dynamics of the sensors and actuators is not neglected. Due to the additional dynamics of the actuators, the passive system described by $\widehat{\mathbf{G}}_{\mathbf{p}}(s)$ is of order twelve. By switching on the active control, this matrix is multiplied by second-order sensor transfer functions $\widehat{\mathbf{G}}_{\mathbf{s}}(s)$ so that the order of the closed loop system is further increased. Thus, the stability analysis using the Routh-Hurwitz criterion becomes rather impractical. Another method of analysing the stability properties of a closed loop system having multiple inputs and outputs (MIMO) is the generalised Nyquist criterion.

### 3.6 MIMO stability analysis

The generalised Nyquist stability criterion may be used to assess the stability of a feedback system with multiple inputs and outputs by analysing the properties of the sensor-actuator open loop FRF. This matrix needs to be inverted, as shown in Eq. (23*b*), and as such needs to be regular in order for the system to remain stable. The generalised Nyquist stability criterion states that the closed loop feedback system is stable if the locus of the following determinant does not encircle the origin of the complex plane as frequency $\omega$ varies from $-\infty$ to $\infty$ [41]:

$$\det\left[\mathbf{I}+\widehat{\mathbf{G}}_{\mathbf{sa}}(\mathrm{j}\omega)\right]=\left[1+\hat{\lambda}_1(\mathrm{j}\omega)\right]\left[1+\hat{\lambda}_2(\mathrm{j}\omega)\right]\left[1+\hat{\lambda}_3(\mathrm{j}\omega)\right]\left[1+\hat{\lambda}_4(\mathrm{j}\omega)\right], \tag{24}$$

$$\widehat{\mathbf{G}}_{\mathbf{sa}}(s)=\widehat{\mathbf{G}}_{\mathbf{s}}(s)\widehat{\mathbf{G}}_{\mathbf{p}}(s)\widehat{\mathbf{G}}_{\mathbf{c}}. \tag{25}$$

In Eq. (24), the fact that the determinant of a matrix is equal to the product of all of its eigenvalues is used. As such, $\hat{\lambda}_i(\mathrm{j}\omega)$ represents the *i*-th eigenvalue of $\widehat{\mathbf{G}}_{\mathbf{sa}}(\mathrm{j}\omega)$, $i$=1...4 [42]. In general, matrix $\widehat{\mathbf{G}}_{\mathbf{sa}}$ has as many eigenvalues as there are feedback loops and thus in the present case the matrix should have two eigenvalues. However, because of the "artificial" expansion of matrix $\widehat{\mathbf{G}}_{\mathbf{c}}$ with zero rows (see Eq. (22*c*)), two of the eigenvalues are constant and equal zero. Only the two non-zero eigenvalues are relevant in the forthcoming stability analysis. Then the standard single-input-single-output Nyquist criterion can be applied to each of the two eigenvalues. In other words, the active metamaterial cell will be stable if neither of the loci of $\hat{\lambda}_1(\mathrm{j}\omega)$ and $\hat{\lambda}_2(\mathrm{j}\omega)$ encircles the Nyquist point –1+0j.

Such a stability analysis is conducted on a system given as an example with parameters shown in Table 3. These parameters have been determined from the experimental setup, which is presented in more detail in Section 4.

**Table 3 Parameters of the active metamaterial cell with included transducer dynamics**

| parameter | value |
|---|---|
| $m_1$ | 0.045 kg |
| $m_2$ | 0.06075 kg |
| $k_1$ | 55400 N $m^{-1}$ |
| $k_2$ | 9100 N $m^{-1}$ |
| $k_{1,2}$ | 18150 N $m^{-1}$ |
| $k_{2,1}$ | 17850 N $m^{-1}$ |
| $c$ | 0.8 N s $m^{-1}$ |
| $T$ | 0.45 N $A^{-1}$, V s $m^{-1}$ |
| $L$ | $63\times10^{-6}$ H |
| $R$ | 1.5 Ω |
| $\omega_m$ | $2\pi\times42\times10^3$ rad $s^{-1}$ |
| $\zeta_m$ | 0.00158 (dimensionless) |
| $\hat{g}$ | 300 V s $m^{-1}$ |

Figure 11 shows the Nyquist contours of both eigenvalues of the sensor-actuator open loop FRF matrix. The thick red line represents the case where the dynamic behaviour of the sensors and actuators is taken into account, whereas the dashed blue line represents the analogous locus when these dynamics are neglected.

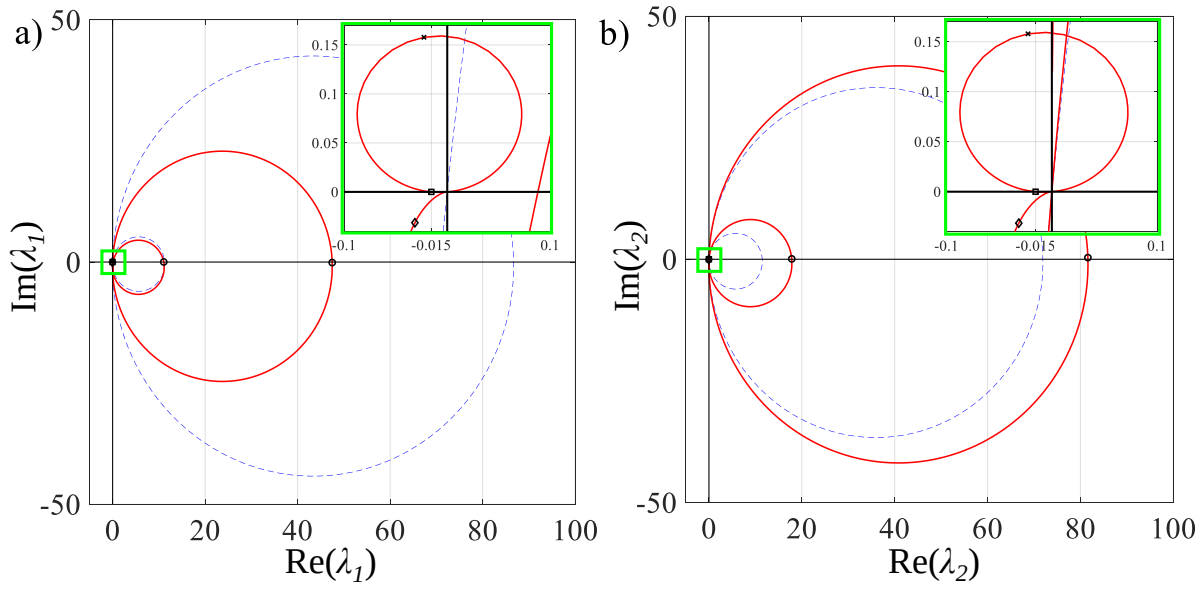


**Figure 11 Nyquist contours of the eigenvalues $\lambda_1$ (a) and $\lambda_2$ (b) of the sensor-actuator open loop frequency response function matrix: model with included sensor-actuator dynamics – solid red line, model with idealised sensors and actuators – dashed blue line (black circles indicate the eigenfrequencies of the system, the black diamond indicates the cut-off frequency of the electrodynamic actuators, the black square indicates the point at which the contour crosses the negative real axis, the black "×" indicates the eigenfrequency of the sensors)**

By considering Figure 11, it can be noticed that the thick red line crosses the negative real axis even though the parameters of the passive system have been chosen so that inequalities (13) and (14) are satisfied (see the zoomed frame in Figure 11). This is in contrast to the case where sensor-actuator dynamics are not taken into account, which demonstrates that in practice, when using realistic transducers, it is not possible to guarantee the unconditional stability but only a certain stability margin. In particular, one can consider the gain margin, which is defined as the distance between the point at which the contour intersects the negative real axis (marked with a black square in Figure 11) and the Nyquist point -1+0j. The value of the chosen feedback gain $\hat{g}$ (see Table 3) ensures quite a large gain margin of about 36 dB. This can be seen by considering the Bode plots of the two eigenvalues, shown in Figure 12 and Figure 13. The mathematical model including sensor-actuator dynamics is denoted by a thick red line, while the case in which idealised transducers are assumed is represented by a dashed blue line.

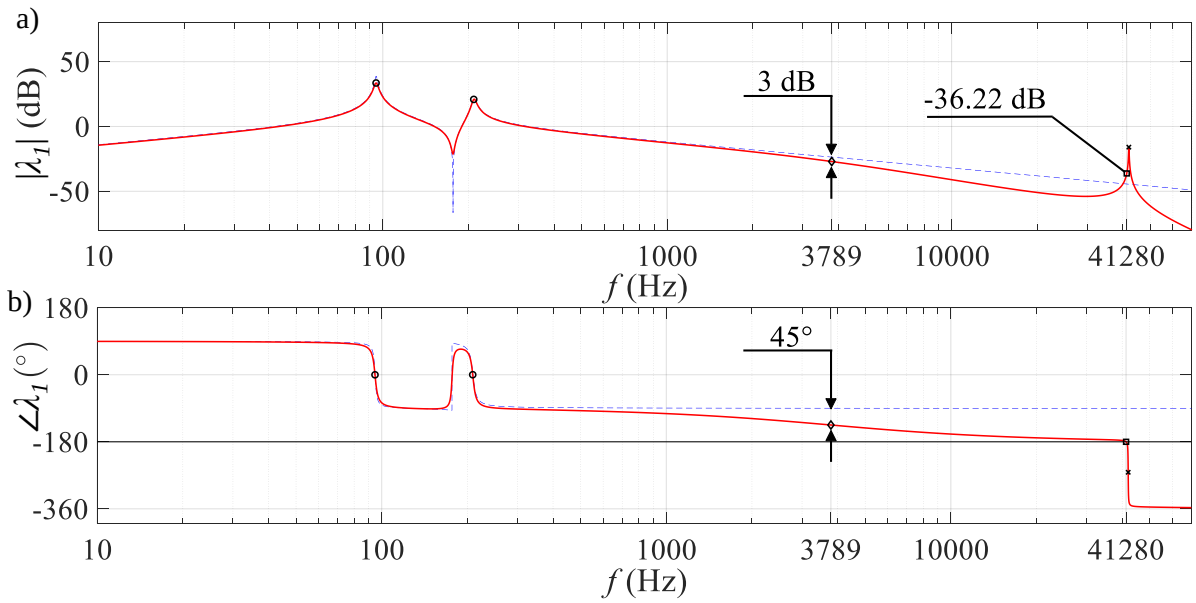


**Figure 12 Amplitude (a) and phase (b) plot of the first eigenvalue ($\lambda_1$) of the sensor-actuator open loop frequency response function matrix: model with included sensor-actuator dynamics – solid red line, model with idealised sensors and actuators – dashed blue line (black circles indicate the eigenfrequencies of the system, the black diamond indicates the cut-off frequency of the electrodynamic actuators, the black square indicates the point at which the contour crosses the negative real axis, the black "×" indicates the eigenfrequency of the sensors)**

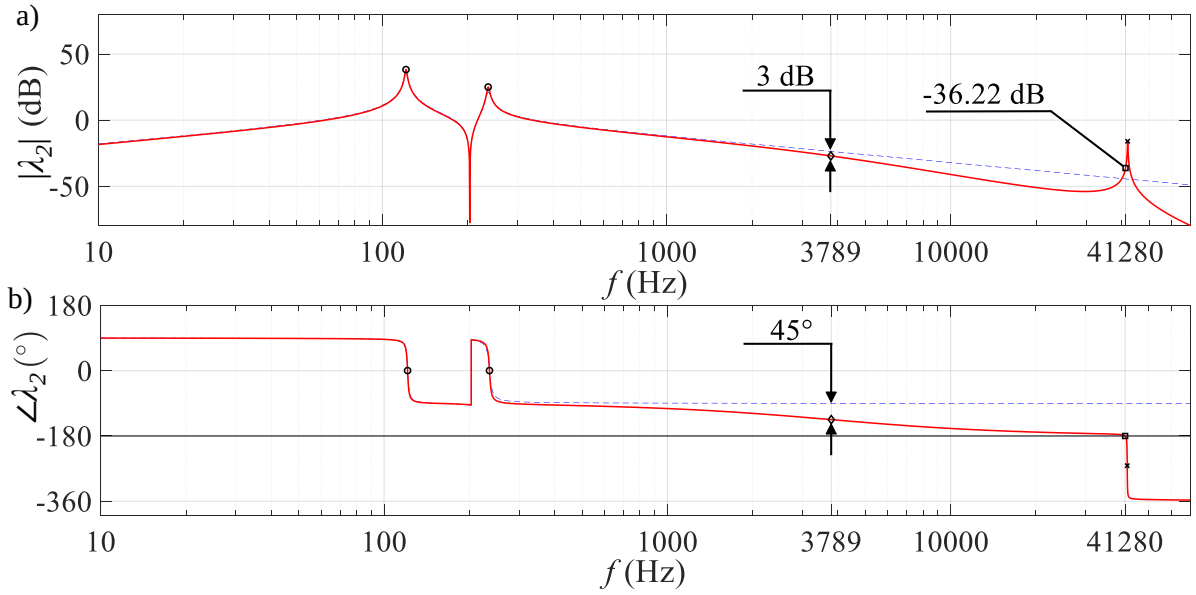


**Figure 13 Amplitude (a) and phase (b) plot of the second eigenvalue ($\lambda_2$) of the sensor-actuator open loop frequency response function matrix: model with included sensor-actuator dynamics – solid red line, model with idealised sensors and actuators – dashed blue line (black circles indicate the eigenfrequencies of the system, the black diamond indicates the cut-off frequency of the electrodynamic actuators, the black square indicates the point at which the contour crosses the negative real axis, the black "×" indicates the eigenfrequency of the sensors)**

Both models yield similar responses up to frequencies of about 1 kHz. The electrodynamic actuators tend to add some passive damping to the system, since electrical current is induced in the electrodynamic

actuators by means of the relative motion of the coil and magnet, and the resistance in the circuit dissipates energy (it behaves like a mechanical damper). Another point of interest is marked with a black diamond and represents the cut-off frequency of the electrical subsystem (the ratio of its resistance and inductance) which is characterised by a drop in gain of 3 dB and phase lag of 45° with respect to the case when the actuator dynamics is not taken into account. Additionally, the model including transducer dynamics has an additional resonance frequency (marked with a black "×" in the figure), which is the blocked mechanical resonance of the seismic accelerometer. It is at a frequency just below this resonance that the phase of the model including transducer dynamics crosses -180°. This can be seen in the Nyquist plot as the crossing of the contour over the negative real axis (indicated by a black square in the figures). At this frequency, the amplitude of both eigenvalues is about -36 dB, which is why 36 dB is considered the gain margin in this case. Given that in practice 6 dB of gain margin is normally sufficient, this model predicts that a larger feedback gain may be implemented. In conclusion, the analysis carried out in this subsection shows that with realistic transducers it is not possible to ensure an unconditional stability system. Nevertheless, the model still predicts quite a large gain margin which may be achieved if the passive system is designed to satisfy inequalities (13) and (14). The next section deals with the experimental validation of the theoretical findings.

# 4 Experimental study

## 4.1 The experimental setup

The design of the experimental setup is shown in Figure 14 a). Note that the setup mimics the lumped parameter model in that the masses are produced by concentrating fairly rigid lumps of material whereas the stiffnesses are produced by lightweight flexible straight or curved beam elements.

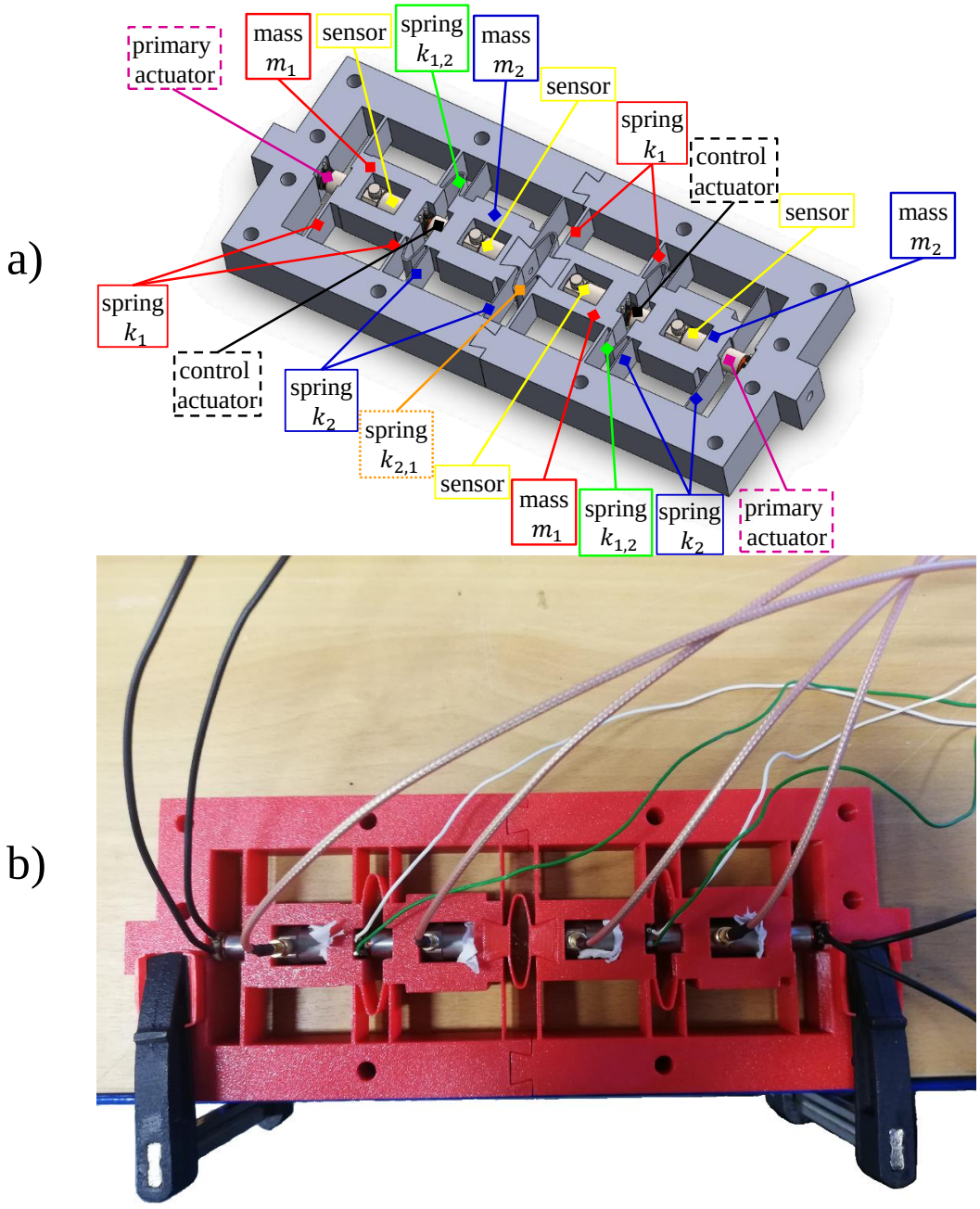


**Figure 14 Active metamaterial experimental setup concept (a) and 3D printed prototype (b)**

Masses $m_1$ and $m_2$ are mimicked by blocks connected via leaf springs (stiffnesses $k_1$ and $k_2$) to a massive frame which is mounted on a rigid foundation. These blocks of material are connected to each other by leaf springs (stiffnesses $k_{1,2}$ and $k_{2,1}$). The colour coding of the elements in Figure 14 a) is identical to the one in Figure 4 and Figure 9 for easier comparison. A significantly greater mass and stiffness of the blocks in comparison to the masses and stiffnesses of the leaf springs ensure that the first four natural frequencies, as well as their corresponding vibration modes, for the most part agree with ones that would be calculated assuming that the springs do not possess inertia and that the blocks were rigid. However, since the parameters of this system are distributed, additional natural modes appear

which cannot be taken into account using the lumped parameter model at frequencies higher than its fourth dominant natural frequency.

The experimental setup is designed while having inequalities (13) and (14) in mind in order to ensure the good stability properties of a closed loop system. This is done by adding extra material to blocks $m_2$ (see Figure 14) to ensure that condition (14) is satisfied. The springs $k_1$ are also made thicker (and thus stiffer) in comparison to springs $k_2$ in order to satisfy inequality (13). A convenient technology for the fabrication of such an experimental setup is 3D printing, as it enables a fast transition from a computer generated model to a physical prototype using a CAD/CAM approach. In particular, a fused deposition modelling printer was used to print the system and PETG (Polyethylene Terephthalate Glycol modified) filament was used as the material. After the printing was complete, the mechanical part of the prototype was equipped with sensors and actuators. This is done according to Figure 14, where the accelerometers are denoted in yellow and are embedded within the rectangular slots into the blocks which represent the four principal moving masses of the system. The electrodynamic actuators used to develop the control forces are denoted in black, and the primary excitation actuators are denoted in magenta. The actuators' properties can be found in Table 3. Likewise, the properties of the seismic accelerometers may be found in the same table.

## 4.2 Measuring equipment and measuring procedures

Figure 15 shows the experimental setup complete with the measuring equipment required for the measurement of the system's response. These include a 4-channel charge amplifier, dynamic signal analyser, power amplifier and a computer. The input to the charge amplifier is the accelerometer signals, which it then amplifies and integrates. In order to implement the proportional controllers, a power amplifier is required to drive the control actuators, which enables the feedback gain to be raised or lowered. This amplifier is also required to adjust the voltage amplitude at the primary actuators used for the excitation of the system. Furthermore, the dynamic signal analyser is used to process all of the signals of interest (the measured velocities and voltages at the terminals of the primary and control actuators) and to generate the white noise excitation signals which were used throughout the study to measure the various FRFs. This type of excitation is chosen to efficiently average out minor nonlinearities in the response of the polymer 3D-printed structure. This method, however, results in a relatively lower signal-to-noise ratio [1]. Nevertheless, the influence of ambient vibration may be mitigated by using an input signal of greater amplitude. In the present case, a white noise signal with root mean square 0.1 V was found to be sufficiently low to provide a satisfactory signal-to-noise ratio without inducing a non-linear structural response. In order to reduce the systematic errors arising from the intrinsic cable EMC noise, coaxial transmission lines in conjunction with robust shielded connectors were used.

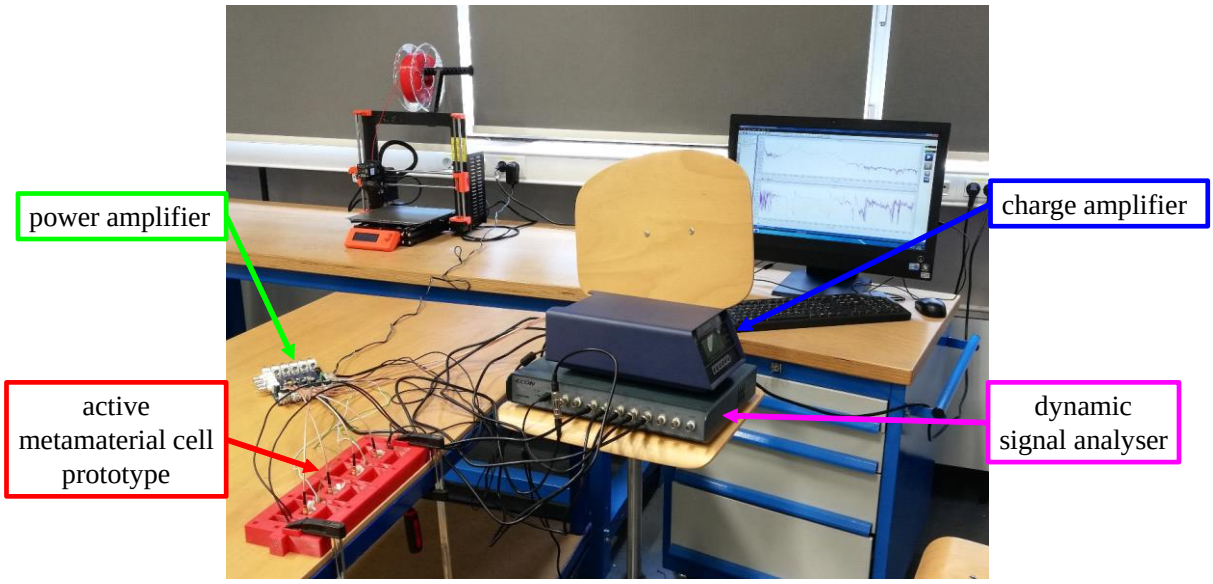


**Figure 15 Experimental setup of the active metamaterial cell prototype complete with measuring equipment**

## 4.3 Experimental stability analysis

Stability is again assessed using the generalised Nyquist criterion. To this end, the sensor-actuator frequency response function matrix must first be assembled. To begin, the responses of the system are measured when it is excited only by the first control actuator (voltage $e_2$), as shown in Figure 16. All the labelling of signals in Figure 16 is the same as in Figure 9 in order to facilitate the comparison of the mathematical model and the experimental setup.

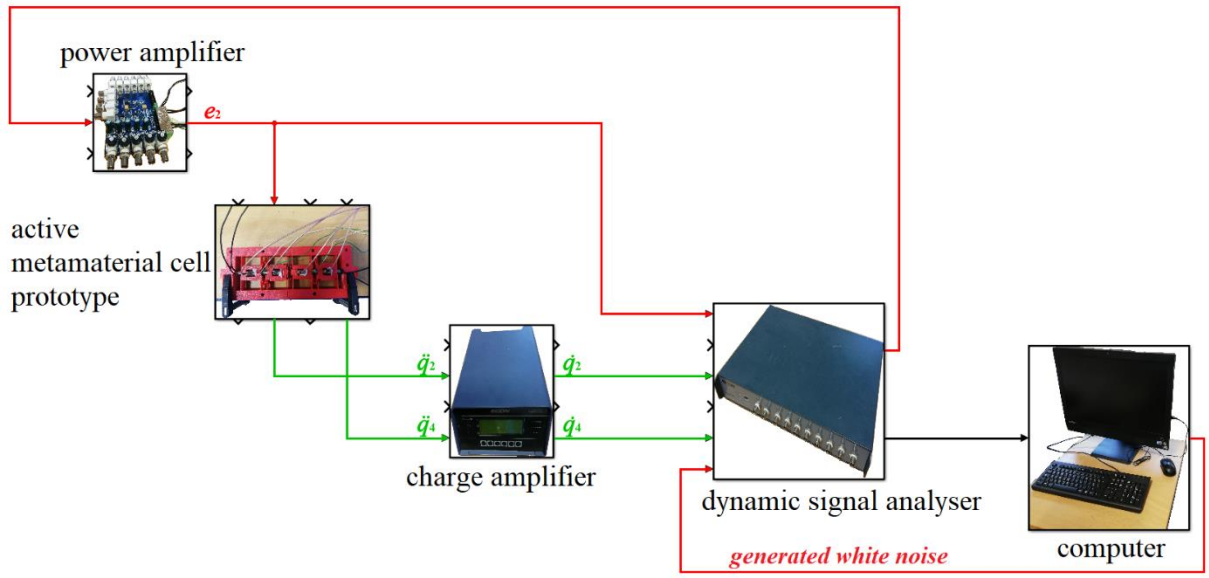


**Figure 16 Measurement of the sensor-actuator frequency response functions when the system is excited with the first feedback actuator**

The red arrow represents the white noise excitation signal, while the green arrows represent the output signal from the accelerometer. The input voltage to the actuator and velocity signals $\dot{q}_2$ and $\dot{q}_4$

are processed in the dynamic signal analyser and are fed to the computer where these data are post processed and saved. The post processing software enables the formation of part of the matrix $\widehat{\mathbf{G}}_{\mathbf{sa}}(\mathrm{j}\omega)$, Eq. (25), with the experimentally obtained data. The same measurement process is repeated with the input voltage at the second feedback actuator $e_3$, after which the entire matrix $\widehat{\mathbf{G}}_{\mathbf{sa}}(\mathrm{j}\omega)$ is populated and one may solve for its eigenvalues at each frequency. Measurements were made up to 24 kHz which is the dynamic signal analyser upper frequency limit. Nyquist contours of the calculated eigenvalues of the sensor-actuator frequency response function matrix are shown in Figure 17.

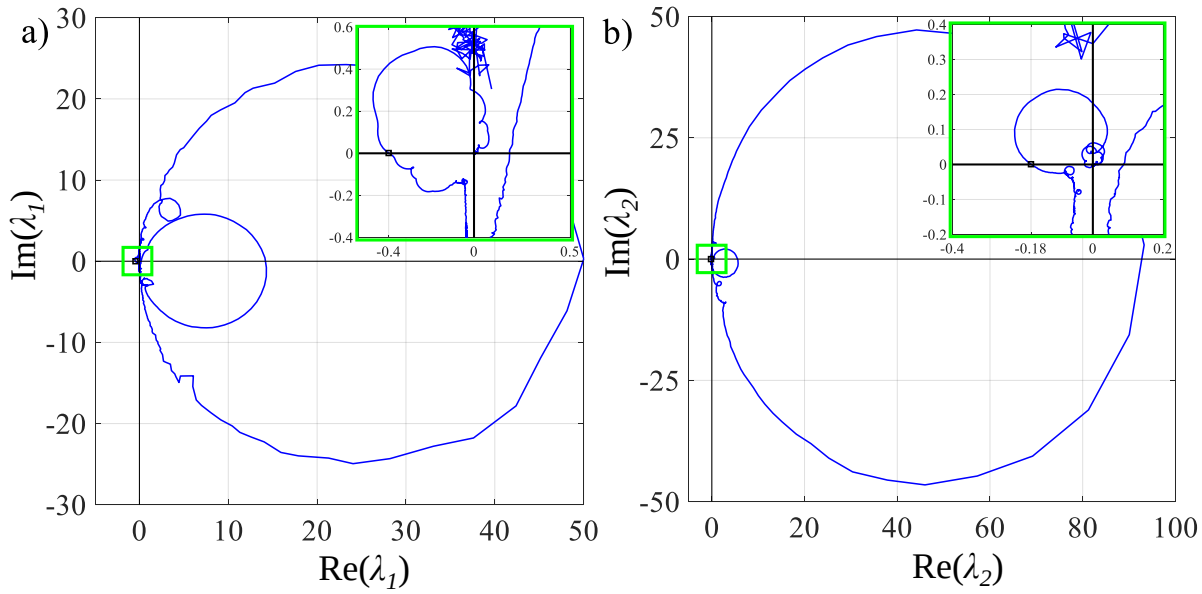


**Figure 17 Nyquist contours of the eigenvalues $\lambda_1$ (a) and $\lambda_2$ (b) of the experimentally obtained sensor-actuator frequency response matrix (the black square indicates the crossing of the contour over the negative real axis)**

Note that the contours intersect the negative real axis at values that are much closer to the Nyquist point, -1+0j, when compared to the case predicted by the mathematical model in the previous section. This indicates a lower stability margin than theoretically anticipated. The stability properties of the system may be better visualised by considering the amplitude and phase plots of the same eigenvalues as shown in Figure 18 and Figure 19 and comparing them to the theoretically predicted ones.

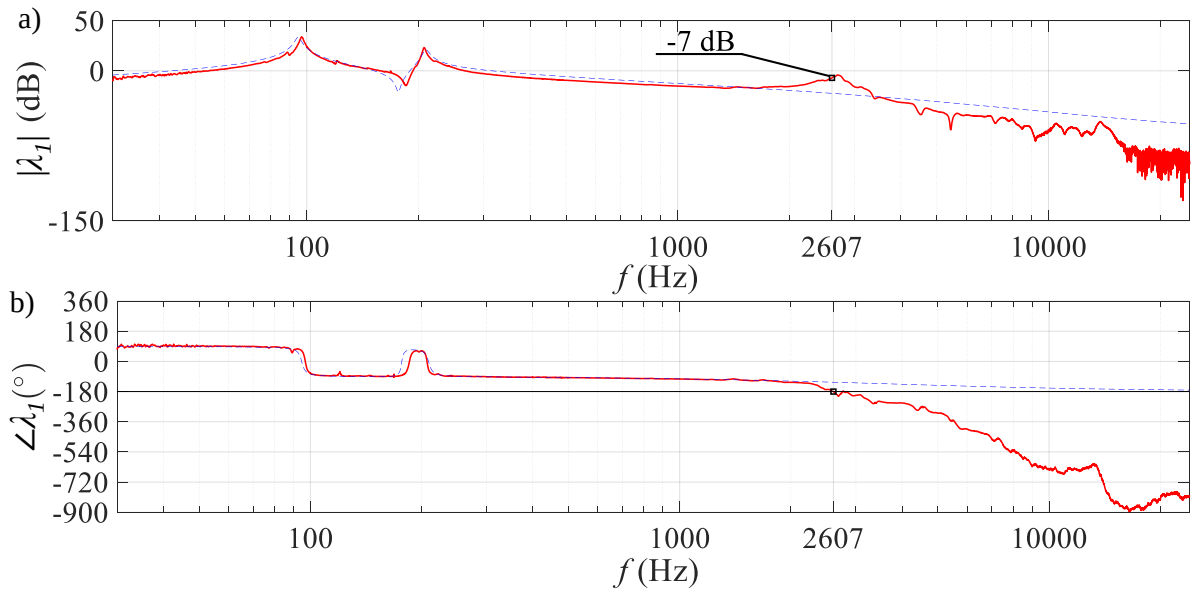


**Figure 18 Amplitude (a) and phase (b) plots of the first eigenvalue of the sensor-actuator frequency response function matrix: mathematical model with included sensor-actuator dynamics – dashed blue line, experimental results – solid red line (the black square indicates the frequency at which the Nyquist contour crosses the negative real axis)**

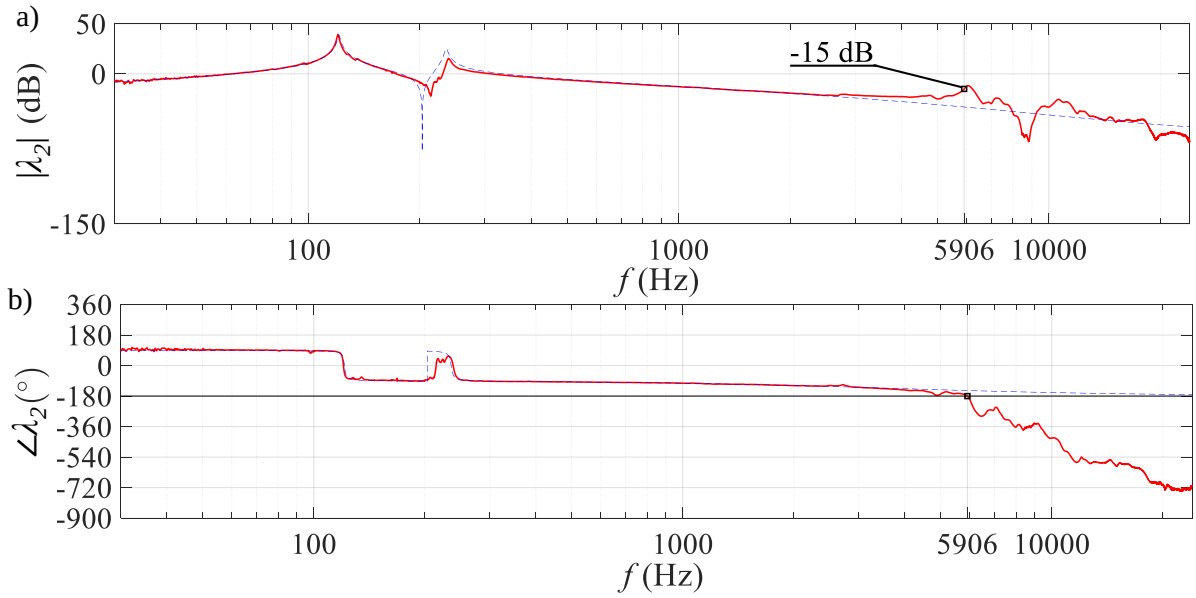


**Figure 19 Amplitude (a) and phase (b) plots of the second eigenvalue of the sensor-actuator frequency response function matrix: mathematical model with included sensor-actuator dynamics – dashed blue line, experimental results – solid red line (the black square indicates the frequency at which the Nyquist contour crosses the negative real axis)**

It can be noticed that the eigenvalues calculated according to the mathematical model and the experimentally obtained ones agree well at low frequencies. However, at frequencies higher than 2 kHz, deviations between the theoretical and experimental eigenvalues occur. This may be explained by the fact that the experimental prototype is a system with distributed parameters which possesses an infinite number of natural frequencies and vibration modes. For this reason, the phase lag of 180° occurs at

much lower frequencies than theoretically predicted and at amplitudes much higher than predicted. In particular, the theoretical model predicts a gain margin of about 36 dB (Figure 12 and Figure 13), while the measured gain margin amounts to about 7 dB (Figure 18). Even though the measured stability margin is much lower than predicted, it is still sufficient, since in practice margins of about 6 dB are often considered satisfactory. This behaviour is caused by a phenomenon known as control spillover. It is present in the vibration control of continuous structures where a finite dimensional controller interacts with residual modes not taken into account during synthesis, but which are present in the physical system. More on this phenomenon and various methods of its compensation may be found in [43] and [44].

The next subsection deals with measurements of the characteristic transfer functions in order to determine how the system transmits vibrations in two of its characteristic directions.

## 4.4 Performance

Given that the analysis from the previous subsection determines that the active metamaterial cell can be made stable with a gain margin of 7 dB, in this section the results of measurements of the two characteristic FRFs, $\hat{G}_{4,1}$ and $\hat{G}_{1,2}$, are presented in order to show how the cell transmits vibrations from its leftmost degree of freedom to the rightmost and vice versa.[1] Measurements are conducted when a) the feedback loops are open and thus the system is passive, and b) when the feedback loops are closed, making the system active, operating with the 7 dB gain margin. Figure 20 shows passive and active FRFs and also shows a comparison between the experimental results with those obtained using the mathematical model including transducer dynamics. Considering the response when the system is passive, it can be concluded that the mathematical model predicts perfectly reciprocal behaviour, since there is only one solid black line (in that case, $\hat{G}_{1,2}$ and $\hat{G}_{4,1}$ are equal). The measurement results show almost identical behaviour, since the dotted green and dash-dotted magenta line almost coincide. This indicates that the passive experimental system exhibits reciprocal behaviour as well, with only minor differences. These differences are due to the differences in the transducers used and minor nonlinearities. When the active control is switched on, these two characteristic transfer functions become rather different, indicating a very large loss of reciprocity. In particular, in the resonance controlled frequency range, the differences between the amplitudes of the characteristic transfer functions case, $\hat{G}_{1,2}$ and $\hat{G}_{4,1}$, reach about 20 dB, whereas this difference in the mass controlled range becomes even larger and reaches 30 dB. Very good agreement is found between the mathematical model and the experimentally obtained results, where the major differences occur only at higher frequencies where the amplitudes are small and the signals approach the noise floor of the measurement chain.

[1] Since the system has two exogenous inputs and four measured outputs, the transfer function matrix $\widehat{\mathbf{G}}$ is a 4×2 matrix, which is why $\hat{G}_{4,1}$ and $\hat{G}_{1,2}$ are the characteristic transfer functions that should be compared (i.e. not $\hat{G}_{4,1}$ and $\hat{G}_{1,4}$).

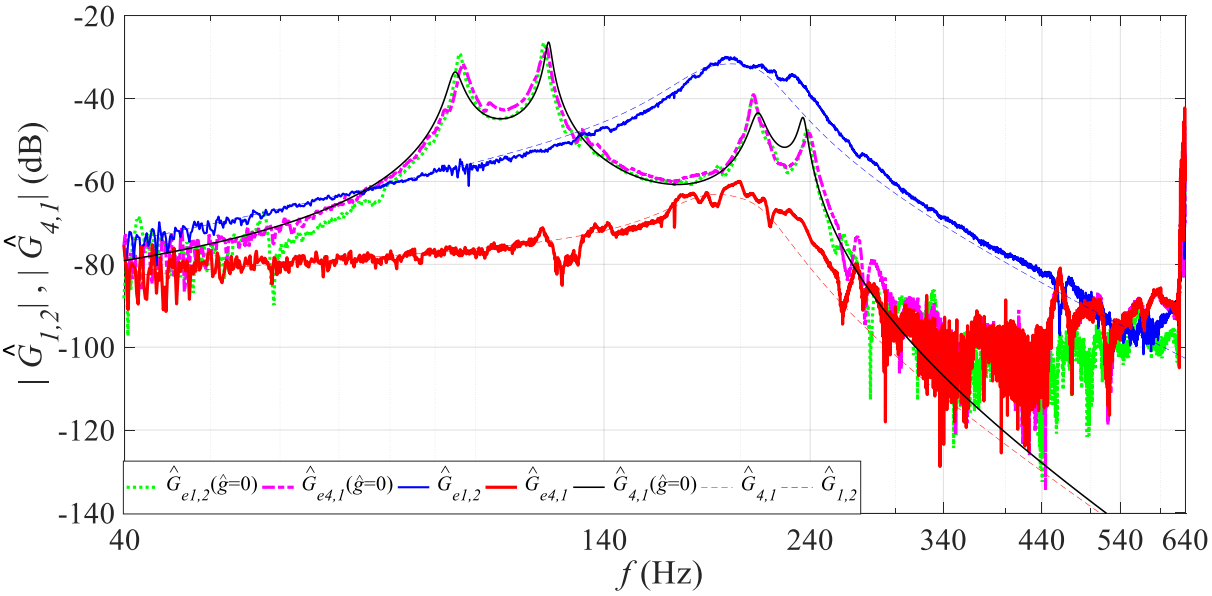


**Figure 20 Comparison between the characteristic transfer functions of the active metamaterial: $\widehat{\boldsymbol{G}}_{\mathbf{1,2}}$ (experimental, passive) – green dotted line, $\widehat{\boldsymbol{G}}_{\mathbf{4,1}}$ (experimental, passive) – magenta dash dotted line, $\widehat{\boldsymbol{G}}_{\mathbf{1,2}} = \widehat{\boldsymbol{G}}_{\mathbf{4,1}}$ (theoretical, passive) – black solid line, $\widehat{\boldsymbol{G}}_{\mathbf{1,2}}$ (experimental, active) – solid blue line, $\widehat{\boldsymbol{G}}_{\mathbf{4,1}}$ (experimental, active) – thick red line, $\widehat{\boldsymbol{G}}_{\mathbf{1,2}}$ (theoretical, active) – faint dashed blue line, $\widehat{\boldsymbol{G}}_{\mathbf{4,1}}$ (theoretical, active) – faint dashed red line**

It can also be noted that the transmission of vibrations when the system is active in the direction left to right according to Figure 14 will be lower at all frequencies when compared to the transmission in the same direction when the system is passive. On the other hand, increased vibration transmission at frequencies higher than 130 Hz is actually facilitated in the opposite direction when the system is made active, so that at these frequencies vibration transmission is amplified when compared to the passive case. In order to better visualise the loss of reciprocity, the experimentally obtained time domain response of the metamaterial cell with white noise input is also given in Figure 21 and Figure 22. Comparing the responses of the metamaterial cell in its opaque and transparent directions, the nonreciprocal response becomes apparent.

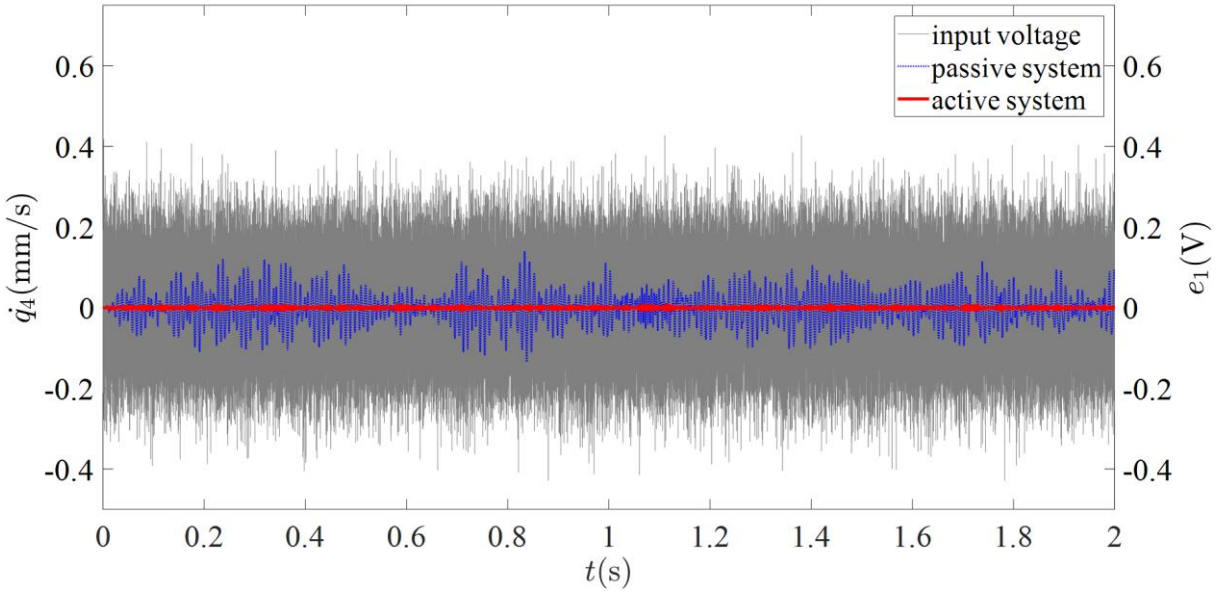


**Figure 21 Time domain response of the active metamaterial cell in the opaque direction**

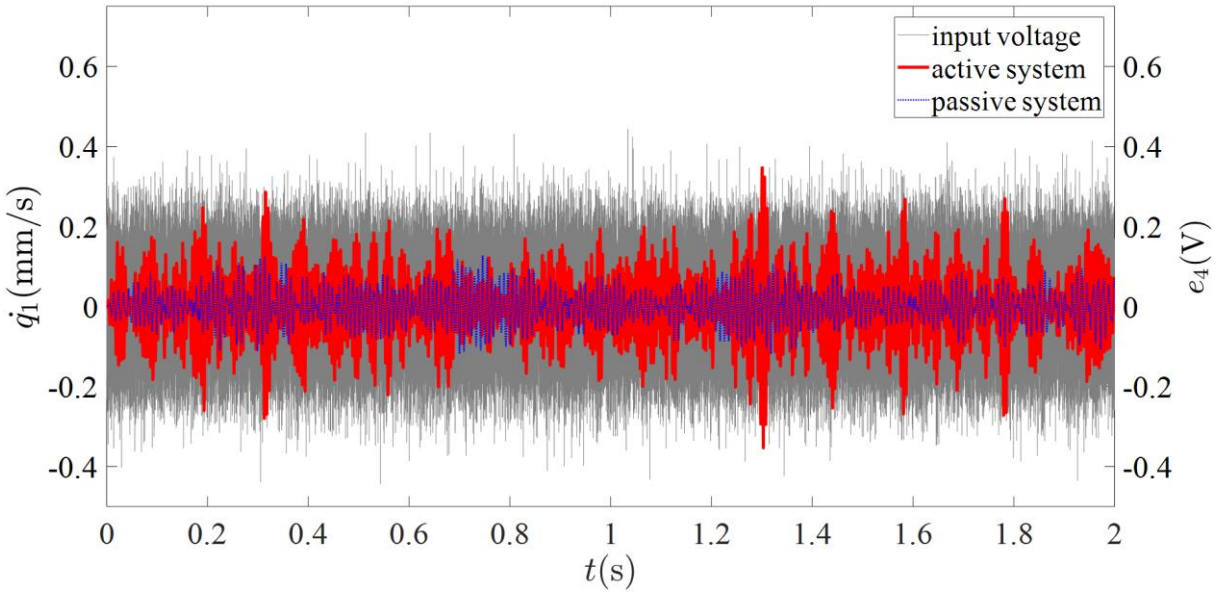


**Figure 22 Time domain response of the active metamaterial cell in the transparent direction**

It would be interesting to consider a proportional-integral (PI) controller to induce a larger reciprocity loss at low frequencies. This is because the responses of mechanical structures below fundamental resonance are stiffness controlled. Then an amount of absolute displacement feedback in addition to the absolute velocity feedback may contribute to disrupting the reciprocity also in the stiffness-controlled low frequency range.

# 5 Conclusions

An active metamaterial concept is introduced, which utilises two non-collocated decentralised velocity feedback loops to achieve a nonreciprocal response of the structure under control. Theoretical analysis of the system neglecting transducer dynamics led to criteria which the passive system should satisfy in order to achieve unconditional stability in a closed loop in terms of two simple inequalities. Augmenting the mathematical model with the sensor-actuator dynamics reveals that these dynamics infringe on the stability properties of the system in a closed loop. Thus, when working with real transducers, it is not possible to guarantee unconditional stability, but rather only ensure a satisfactory stability margin. Theoretical predictions are validated by measurements carried out using an experimental prototype. A significant difference in vibration transmission in the two opposing directions is measured. This difference increases with frequency and is of the order 20-30 dB, which shows that a significant loss of reciprocity may be achieved by using the proposed control scheme. Good agreement between the theoretical and the experimental results is found at frequencies below approximately 340 Hz. Some differences are however found at higher frequencies. These can be explained by the influence of residual higher-order modes which are neglected in the theoretical model. Potential improvement to the stability properties of the system may be the synthesis of a spillover compensator. The overall results indicate that multiple feedback loops in a non-collocated configuration may be used in the design of active acoustic metamaterials: devices to enable the significantly different transmission of sound depending on the direction it enters such a system.


# Acknowledgement

This work has been supported by the Croatian Science Foundation under project no. IP-2019-04-5402. Goran Radan, dipl. ing., is gratefully acknowledged for the design of the power amplifier used in the experimental study.

## References


[1] W. Heylen, S. Lammens, P. Sas, Modal Analysis Theory and Testing, Katholieke Universiteit Leuven, Faculty of Engineering, Department of Mechanical Engineering, Division of Production Engineering, Machine Design and Automation, 1998.

[2] B.S. Kim, G.J. Kim, T.K. Lee, The identification of tyre induced vehicle interior noise, Appl. Acoust. 68 (2007) 134–156. https://doi.org/10.1016/j.apacoust.2006.05.020.

[3] J.T. Fokkema, P.M. van den Berg, Seismic Applications of Acoustic Reciprocity, Elsevier, 1993. https://doi.org/10.1016/C2009-0-10209-X.

[4] R. Fleury, D.L. Sounas, C.F. Sieck, M.R. Haberman, A. Alù, Sound isolation and giant linear nonreciprocity in a compact acoustic circulator, Science (80-. ). 343 (2014) 516–519. https://doi.org/10.1126/science.1246957.

[5] D.L. Sounas, C. Caloz, A. Alù, Giant non-reciprocity at the subwavelength scale using angular momentum-biased metamaterials, Nat. Commun. 4 (2013) 2407. https://doi.org/10.1038/ncomms3407.

[6] A. Kamal, J. Clarke, M.H. Devoret, Noiseless non-reciprocity in a parametric active device, Nat. Phys. 7 (2011) 311–315. https://doi.org/10.1038/nphys1893.

[7] B.I. Popa, S.A. Cummer, Nonreciprocal active metamaterials, Phys. Rev. B - Condens. Matter Mater. Phys. 85 (2012) 1–6. https://doi.org/10.1103/PhysRevB.85.205101.

[8] R. Fleury, D. Sounas, A. Alù, An invisible acoustic sensor based on parity-time symmetry, Nat. Commun. 6 (2015) 1–7. https://doi.org/10.1038/ncomms6905.

[9] C. House, J. Cheer, S. Daley, An experimental investigation into active structural acoustic cloaking of a flexible cylinder, Appl. Acoust. 170 (2020) 107436. https://doi.org/10.1016/j.apacoust.2020.107436.

[10] N. Alujević, I. Senjanović, I. Ćatipović, N. Vladimir, The absence of reciprocity in active structures using direct velocity feedback, J. Sound Vib. 438 (2018) 251–256. https://doi.org/10.1016/j.jsv.2018.09.035.

[11] L. Sirota, F. Semperlotti, A.M. Annaswamy, Tunable and reconfigurable mechanical transmission-line metamaterials via direct active feedback control, Mech. Syst. Signal Process. 123 (2019) 117–130. https://doi.org/10.1016/j.ymssp.2019.01.001.

[12] J. Tan, J. Cheer, S. Daley, Realisation of nonreciprocal transmission and absorption using wave-based active noise control, JASA Express Lett. 2 (2022) 054801. https://doi.org/10.1121/10.0010454.

[13] H. Nassar, B. Yousefzadeh, R. Fleury, M. Ruzzene, A. Alù, C. Daraio, A.N. Norris, G. Huang, M.R. Haberman, Nonreciprocity in acoustic and elastic materials, Nat. Rev. Mater. 5 (2020) 667–685. https://doi.org/10.1038/s41578-020-0206-0.

[14] S.A. Cummer, J. Christensen, A. Alù, Controlling sound with acoustic metamaterials, Nat. Rev. Mater. 1 (2016) 16001. https://doi.org/10.1038/natrevmats.2016.1.

[15] F. Zangeneh-Nejad, R. Fleury, Active times for acoustic metamaterials, Rev. Phys. 4 (2019) 100031. https://doi.org/10.1016/j.revip.2019.100031.

[16] B.Y. Hu, Kramers–Kronig in two lines, Am. J. Phys. 57 (1989) 821–821. https://doi.org/10.1119/1.15901.

[17] C. Claeys, N.G. Rocha de Melo Filho, L. Van Belle, E. Deckers, W. Desmet, Design and validation of metamaterials for multiple structural stop bands in waveguides, Extrem. Mech. Lett. 12 (2017) 7–22. https://doi.org/10.1016/j.eml.2016.08.005.

[18] L. Sangiuliano, B. Reff, J. Palandri, F. Wolf-Monheim, B. Pluymers, E. Deckers, W. Desmet, C. Claeys, Low frequency tyre noise mitigation in a vehicle using metal 3D printed resonant metamaterials, Mech. Syst. Signal Process. 179 (2022) 109335. https://doi.org/10.1016/j.ymssp.2022.109335.

[19] L.Y.M. Sampaio, G.K. Rodrigues, J.A. Mosquera-Sánchez, C. De Marqui, L.P.R. de Oliveira,

Membrane smart metamaterials for unidirectional wave propagation problems, J. Sound Vib. 512 (2021) 116374. https://doi.org/10.1016/j.jsv.2021.116374.
[20] Q. Xu, J. Qiao, J. Sun, G. Zhang, L. Li, A tunable massless membrane metamaterial for perfect and low-frequency sound absorption, J. Sound Vib. 493 (2021) 115823. https://doi.org/10.1016/j.jsv.2020.115823.
[21] H. Nassar, H. Chen, A.N. Norris, M.R. Haberman, G.L. Huang, Non-reciprocal wave propagation in modulated elastic metamaterials, Proc. R. Soc. A Math. Phys. Eng. Sci. 473 (2017) 20170188. https://doi.org/10.1098/rspa.2017.0188.
[22] K. Yi, M. Ouisse, E. Sadoulet-Reboul, G. Matten, Active metamaterials with broadband controllable stiffness for tunable band gaps and non-reciprocal wave propagation, Smart Mater. Struct. 28 (2019). https://doi.org/10.1088/1361-665X/ab19dc.
[23] D.H. Sheingold, Impedance & admittance transformations using operational amplifiers, Light. Empiricist. 12 (1964) 1–8.
[24] C.M. Bender, S. Boettcher, Real spectra in Non-Hermitian Hamiltonians having PT symmetry, Phys. Rev. Lett. 80 (1998) 5243–5246. https://doi.org/10.1103/PhysRevLett.80.5243.
[25] J. Christensen, M. Willatzen, V.R. Velasco, M.-H. Lu, Parity-time synthetic phononic media, Phys. Rev. Lett. 116 (2016) 207601. https://doi.org/10.1103/PhysRevLett.116.207601.
[26] M. Zilletti, P. Gardonio, S.J. Elliott, Optimisation of a velocity feedback controller to minimise kinetic energy and maximise power dissipation, J. Sound Vib. 333 (2014) 4405–4414. https://doi.org/10.1016/j.jsv.2014.04.036.
[27] J. Lončar, J. Vuković, I. Krois, S. Hrabar, Stability constraints on practical implementation of parity-time-symmetric electromagnetic systems, Photonics. 8 (2021) 56. https://doi.org/10.3390/photonics8020056.
[28] M.G. Tehrani, J.E. Mottershead, An overview of the receptance method in active vibration control, IFAC Proc. Vol. 45 (2012) 1174–1178. https://doi.org/10.3182/20120215-3-AT-3016.00208.
[29] J.E. Mottershead, M.G. Tehrani, S. James, Y.M. Ram, Active vibration suppression by pole-zero placement using measured receptances, J. Sound Vib. 311 (2008) 1391–1408. https://doi.org/10.1016/j.jsv.2007.10.024.
[30] S. Chesné, C. Collette, Experimental validation of fail-safe hybrid mass damper, JVC/Journal Vib. Control. 24 (2018) 4395–4406. https://doi.org/10.1177/1077546317724949.
[31] J. Rohlfing, S.J. Elliott, P. Gardonio, Compensation Filter for Feedback Control Units with Proof-Mass Electrodynamic Actuators, Simulations and Experimental Studies, Southampton, 2011.
[32] C. Collette, S. Chesné, Robust hybrid mass damper, J. Sound Vib. 375 (2016) 19–27. https://doi.org/10.1016/j.jsv.2016.04.030.
[33] Y. Gao, L. Wang, Nonlocal active metamaterial with feedback control for tunable bandgap and broadband nonreciprocity, Int. J. Mech. Sci. 219 (2022) 107131. https://doi.org/10.1016/j.ijmecsci.2022.107131.
[34] S. Elliot, Signal Processing for Active Control, Elsevier, 2001. https://doi.org/10.1016/B978-0-12-237085-4.X5000-5.
[35] G.J. Balas, J.C. Doyle, Collocated versus non-collocated multivariable control for flexible structure, in: 1990 Am. Control Conf., IEEE, 1990: pp. 1923–1928. https://doi.org/10.23919/ACC.1990.4791064.
[36] N. Alujević, H. Wolf, P. Gardonio, I. Tomac, Stability and performance limits for active vibration isolation using blended velocity feedback, J. Sound Vib. 330 (2011) 4981–4997. https://doi.org/10.1016/j.jsv.2011.05.020.
[37] O.N. Baumann, S.J. Elliott, The stability of decentralized multichannel velocity feedback controllers using inertial actuators, J. Acoust. Soc. Am. 121 (2007) 188–196. https://doi.org/10.1121/1.2400674.
[38] A. Caiazzo, N. Alujević, B. Pluymers, W. Desmet, Active control of turbulent boundary layer sound transmission into a vehicle interior, J. Phys. Conf. Ser. 744 (2016). https://doi.org/10.1088/1742-6596/744/1/012026.
[39] Z. Ge, W. Wang, G. Li, D. Rao, Design, parameter optimisation, and performance analysis of active tuned inerter damper (TID) suspension for vehicle, J. Sound Vib. 525 (2022) 116750.

https://doi.org/10.1016/j.jsv.2022.116750.
[40] K. Zhou, J.C. Doyle, K. Glover, Robust and Optimal Control, Prentice Hall, 1996.
[41] S. Skogestad, Multivariable Feedback Control: Analysis and Design, John Wiley, 2007. https://doi.org/10.1002/(SICI)1099-1239(19981215)8:14<1237::AID-RNC377>3.0.CO;2-7.
[42] C.G. Díaz, C. Paulitsch, P. Gardonio, Smart panel with active damping units. Implementation of decentralized control, J. Acoust. Soc. Am. 124 (2008) 898–910. https://doi.org/10.1121/1.2945168.
[43] M.J. Balas, Direct velocity feedback control of large space structures, J. Guid. Control. Dyn. 2 (1979) 252–253. https://doi.org/10.2514/3.55869.
[44] W. Liu, Vibration control of large scale flexible structures using magnetorheological dampers, Worcester Polytechnic Institute, 2005.